

1 **The Early Toarcian oceanic anoxic event: Paleoenvironmental and paleoclimatic change**
2 **across the Alpine Tethys (Switzerland)**

3 Alicia Fantasia^{1*}, Karl B. Föllmi¹, Thierry Adatte¹, Jorge E. Spangenberg², Jean-Carlos
4 Montero-Serrano^{3,4}

5 ¹ *Institute of Earth Sciences (ISTE), University of Lausanne, 1015 Lausanne, Switzerland (*corresponding author:*
6 *alicia.fantasia@unil.ch)*

7 ² *Institute of Earth Surface Dynamics (IDYST), University of Lausanne, 1015 Lausanne, Switzerland*

8 ³ *Marine Sciences Institute (ISMER), University of Quebec in Rimouski, Rimouski, Quebec, G5L 3A1, Canada*

9 ⁴ *GEOTOP Research Center, C.P. 8888, Montreal, QC H3C 3P8, Canada*

10

11 **Abstract**

12 Paleoenvironmental and paleoclimatic change associated with the Toarcian oceanic
13 anoxic event (T-OAE) was evaluated in five successions located in Switzerland. They
14 represent different paleogeographic settings across the Alpine Tethys: the northern shelf
15 (Gipf, Riniken and Rietheim), the Sub-Briançonnais basin (Creux de l'Ours), and the
16 Lombardian basin (Breggia). The multi-proxy approach chosen (whole-rock and clay
17 mineralogy, phosphorus, major and trace elements) shows that local environmental conditions
18 modulated the response to the T-OAE across the Alpine Tethys. On the northern shelf and in
19 the Sub-Briançonnais basin, high kaolinite contents and detrital proxies (detrital index, Ti, Zr,
20 Si) in the T-OAE interval suggest a change towards a warmer and more humid climate
21 coupled with an increase in the chemical weathering rates. In contrast, low kaolinite content
22 in the Lombardian basin is likely related to a more arid climate along the southern Tethys
23 margin and/or to a deeper and more distal setting. Redox-sensitive trace-element (V, Mo, Cu,
24 Ni) enrichments in the T-OAE intervals reveal that dysoxic to anoxic conditions developed on
25 the northern shelf, whereas reducing conditions were less severe in the Sub-Briançonnais

26 basin. In the Lombardian basin well-oxygenated bottom water conditions prevailed.
27 Phosphorus (P) speciation analysis was performed at Riniken and Creux de l'Ours. This is the
28 first report of P speciation data for T-OAE sections, clearly suggesting that high P contents
29 during this time interval are mainly linked to the presence of an authigenic phases and fish
30 remains. The development of oxygen-depleted conditions during the T-OAE seems to have
31 promoted the release of the organic-bound P back into the water column, thereby further
32 sustaining primary productivity in a positive feedback loop.

33

34 **Keywords:** Toarcian OAE; Proximal-distal transect; Mineralogy; Geochemistry; Phosphorus;
35 Climate change

36

37 **1. Introduction**

38 The Toarcian oceanic anoxic event (T-OAE, Early Jurassic) was marked by global
39 warming, a perturbation of the carbon cycle, marine mass extinctions, and the widespread
40 deposition of organic-rich strata, reflecting oceanic anoxia ([Harries and Little, 1999](#); [Jenkyns,](#)
41 [1988](#)). The T-OAE coincides with the onset of the Karoo-Ferrar large igneous province (LIP)
42 and the associated massive pulse in volcanic activity is currently thought to have initiated
43 these environmental and climatic changes ([Pálffy and Smith, 2000](#); [Bond and Wignall, 2014](#);
44 [Burgess et al., 2015](#)). The concomitant marked negative carbon-isotope excursion (CIE)
45 recorded in the *tenuicostatum-falciferum* ammonite zones (or equivalents) was attributed to
46 the injection of isotopically light carbon into the atmosphere and the ocean from (i) the input
47 of thermogenic carbon dioxide (CO₂) produced by interaction of Karoo-Ferrar basalts and
48 organic-rich sediments, (ii) the release of methane from the dissociation of marine clathrates,

49 and (iii) the input of volcanogenic CO₂ (McElwain et al., 2005; Svensen et al., 2007; Kemp et
50 al., 2011). The negative CIE is superimposed on a long-term positive trend, which was
51 interpreted to reflect enhanced organic-carbon burial (Jenkyns, 1988). The negative CIE is
52 recorded in marine carbonate carbon, and terrestrial and marine organic carbon in globally
53 distributed settings, thereby confirming the global nature of the carbon-cycle perturbation and
54 providing a better time marker for the T-OAE than solely the occurrence of organic-rich
55 sediments (e.g., Röhl et al., 2001; Hesselbo et al., 2007; Suan et al., 2011, 2015; Gröcke et al.,
56 2011; Caruthers et al., 2011; Kemp and Izumi, 2014; Reolid 2014; Montero-Serrano et al.,
57 2015; Bodin et al., 2016; Al-Suwaidi et al., 2016; Them II et al., 2017; Xu et al., 2017).
58 Furthermore, global warming strengthened the hydrological cycle, resulting in increased
59 continental weathering and hence higher nutrient fluxes into the oceans (Cohen et al., 2004;
60 Hermoso and Pellenard, 2014; Brazier et al., 2015; Fu et al., 2017). These conditions boosted
61 primary productivity, which led to the development of oxygen-depleted conditions through
62 organic-matter (OM) oxidation (Jenkyns et al., 2010). Hitherto, a major focus of T-OAE
63 studies was on European restricted epicontinental basins and their organic-rich successions
64 (e.g., Baudin et al., 1990; Jenkyns et al., 2001; Röhl et al., 2001; Hermoso et al., 2012). There,
65 OM preservation was fostered by the thermohaline stratification caused by enhanced
66 freshwater input and the southward flux of brackish water from the Laurasian Seaway
67 (Bjerrum et al., 2001; Dera and Donnadieu, 2012). Relatively few studies, however, addressed
68 the geographical extend of anoxic conditions, and the role of productivity and preservation in
69 open-ocean successions (e.g., Gröcke et al., 2011; Them II et al., 2017).

70 In this study, a high-resolution multi-proxy study was performed on five Lower
71 Toarcian successions located in Switzerland. They represent different paleogeographic
72 settings across the Alpine Tethys, namely its northern shelf (Gipf, Riniken, Rietheim), the
73 Sub-Briançonnais basin (Creux de l'Ours), and the Lombardian basin (Breggia) (Fig. 1). The

74 main purposes of this study were to (i) trace the evolution of environmental and climate
75 change during the T-OAE across the Alpine Tethys, (ii) evaluate the response to the T-OAE
76 of successions deposited in different paleogeographic settings and at different paleodepths,
77 (iii) better constrain the driving mechanisms in the development of oxygen-depleted
78 conditions across the Alpine Tethys, and iv) better understand P behaviour during the T-OAE
79 using P speciation analysis. This is the first report of P speciation values for T-OAE sections,
80 which combined with the other proxies, brings new insight into the impact of the T-OAE and
81 the role of local conditions in modulating the response to this global event.

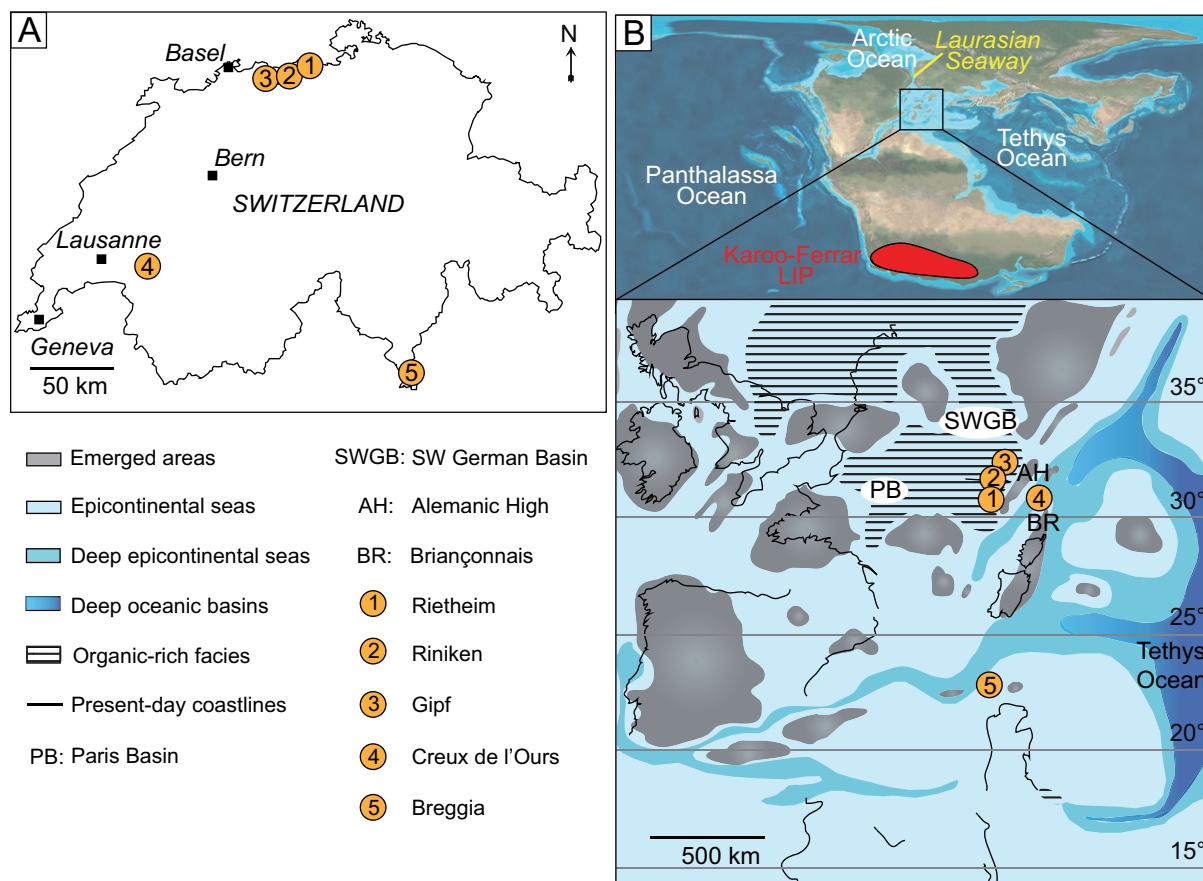
82

83 **2. Geological setting**

84 The successions were selected according to their paleogeographic position and the
85 presence of the negative CIE, which permits to trace the T-OAE interval across the Alpine
86 Tethys (Fig. 1). This was provided by previous lithostratigraphic and biostratigraphic
87 investigations performed by Rieber (1973), Wiedenmayer, (1980), Tröster (1987), Matter et
88 al. (1987), Kuhn and Etter (1994), Mettraux et al. (1989). In addition, a detailed study based
89 on sedimentological features, nannofossil biostratigraphy, organic matter content, and stable
90 isotopes was performed on these successions by Fantasia et al. (in review). This study
91 highlights the presence of numerous stratigraphic gaps and condensed intervals related to the
92 presence of winnowing events and sediment reworking during the T-OAE interval.

93 The sections of Gipf, Riniken (NAGRA borehole) and Rietheim are located in the
94 northern Swiss Tabular Jura (Fig. 1A), canton Aargau, and were selected to characterise the
95 northern shelf of the Alpine Tethys (Fig. 1B; Thierry et al., 2000). The Upper Pliensbachian
96 interval is composed of phosphatic, glauconitic and fossil-rich marl and concretionary marly
97 limestone. The Lower Toarcian interval is characterised by organic-rich laminated marl

98 grading into bioturbated grey marl in the most expanded sections. The T-OAE interval is
99 characterised by organic-rich laminated marl and shows evidences of episodic hydrodynamic
100 conditions. At Gipf, the organic-rich laminated marl is topped by a condensed limestone bed.
101 The *variabilis* and *thouarsense* zones (Middle and Upper Toarcian) are characterised by
102 phosphatic concretionary marl with fossil accumulations (Fig. 2). Previous geochemical and
103 whole-rock mineralogical investigations were recently performed for the Rietheim section by
104 [Montero-Serrano et al. \(2015\)](#). Their results show that the T-OAE interval was characterised
105 by anoxic (possibly euxinic) conditions, authigenic P, and an increase of the continental
106 weathering. This was complement here by clay-minerals data to better constrain the role of
107 climate conditions in modulating the environmental change. In addition, the sections of Gipf
108 and Riniken were chosen in the same area to extend the research to a basin scale and to better
109 understand the role of P during the T-OAE, as it was highlighted in studies on other OAEs
110 (e.g., [Mort et al., 2007](#); [Westermann et al., 2013](#)).

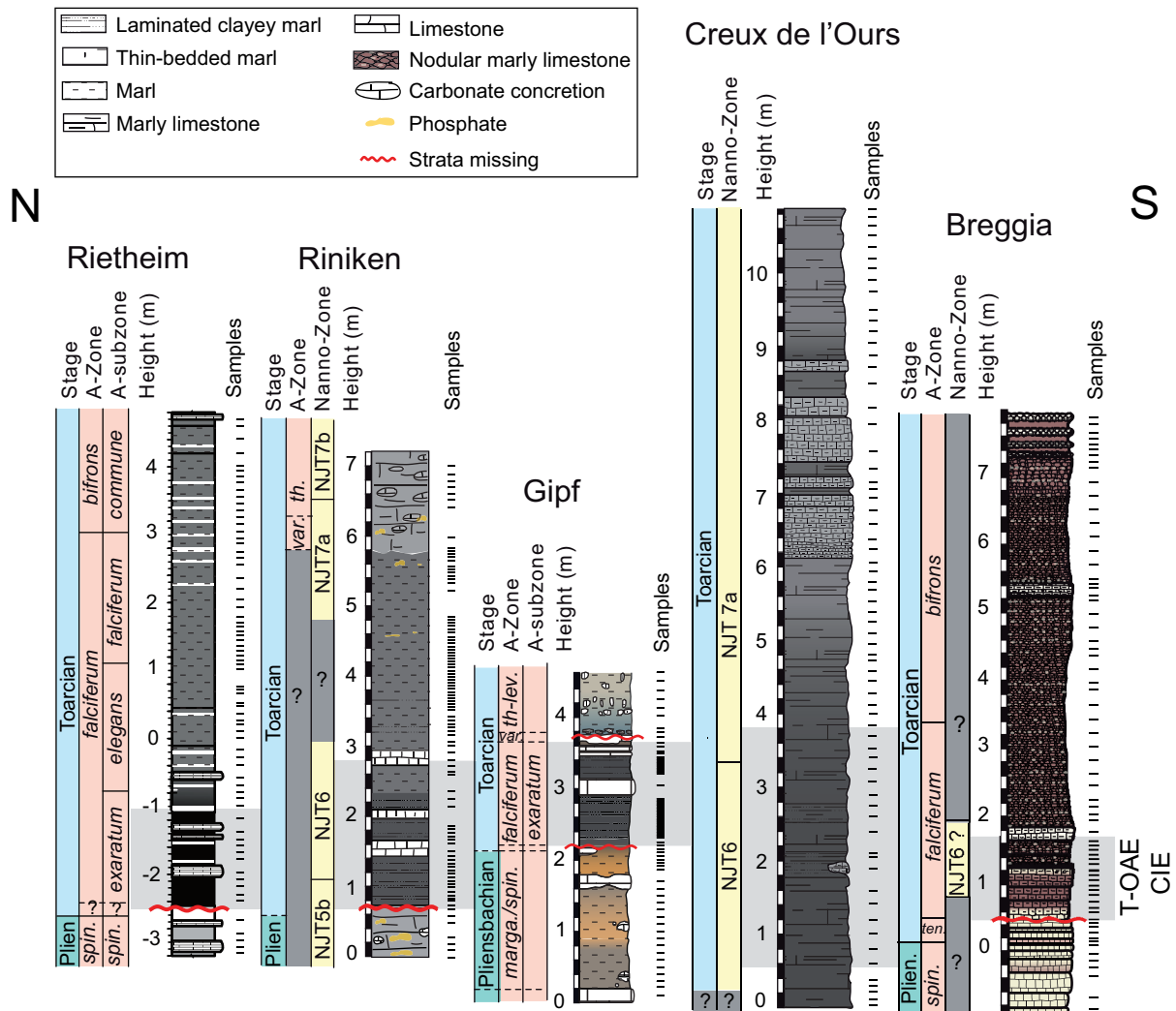


111

112 **Fig. 1.** A) Localisation of the studied sections in Switzerland. B) Paleogeographic map (modified from R. Blakey,
 113 <http://cpgeosystems.com/euromaps.html>) of the Early Toarcian showing the location of the Karoo-Ferrar LIP, the Laurasian
 114 Seaway, and a zoom on the western Tethys (after Thierry et al., 2000) with the location of the studied sections: Gipf,
 115 Riniken, Rietheim, Creux de l'Ours, and Breggia.

116

117 The Creux de l'Ours section is situated in the Préalpes Médiannes Plastiques, canton
 118 Fribourg. The studied sediments were deposited in the Sub-Briançonnais basin, which was
 119 located to the NW of the Briançonnais micro-continent (Fig. 1B; Thierry et al., 2000). The
 120 Toarcian interval (Fig. 2) consists of grey thin-bedded hemipelagic marl and marly limestone
 121 including carbonate concretions formed around accumulations of ostracods and gastropods
 122 shells (*Coelodiscus minutus*). The T-OAE interval consists of thin-bedded marl and records
 123 short episodes of higher hydrodynamic conditions.



124

125 **Fig. 2.** Stratigraphic correlation between the studied sections and lithologies. The Rietheim section is from [Montero-Serrano](#)
 126 [et al. \(2015\)](#).

127

128 The Breggia section is exposed in the southern Alps, Canton Ticino, and was selected
 129 to characterise the hemipelagic realm ([Fig. 1B](#); [Thierry et al., 2000](#)). The sediments from
 130 Breggia were deposited in the Monte Generoso subbasin, which was part of the Lombardian
 131 basin ([Winterer and Bosellini, 1981](#)). The Pliensbachian-Toarcian interval consists of yellow-
 132 grey to reddish bioturbated limestone, which grades into reddish nodular limestone and marl
 133 ([Fig. 2](#)). The T-OAE interval show organic-lean limestone, but the lower part of the interval is
 134 missing because of a stratigraphic gap ([Wiedenmayer, 1980](#)).

135

136 3. Methods

137 A detailed sampling was performed on the sections and whole-rock powders were
138 obtained using an agate crusher. A total of 84 samples were collected at Gipf, 96 at Riniken,
139 65 at Creux de l'Ours and 74 at Breggia (Fig. 2). At Rietheim, 60 samples were selected for
140 clay mineralogy analyses to complement previous geochemical study performed by [Montero-](#)
141 [Serrano et al. \(2015\)](#). Mineralogical and geochemical analyses were conducted at the Institute
142 of Earth Sciences of the University of Lausanne (Switzerland).

143

144 3.1. Whole-rock and clay mineralogy

145 Whole-rock and clay mineralogical analyses were performed on marl and limestone
146 samples using a Thermo Scientific ARL X-TRA Diffractometer. The whole-rock
147 mineralogical composition was semi-quantified using external standards and following the
148 method described by [Klug and Alexander \(1974\)](#), [Kübler \(1987\)](#) and [Adate et al. \(1996\)](#). For
149 the clay minerals, the granulometric fraction $<2 \mu\text{m}$ was obtained following [Kübler, \(1983\)](#)
150 and [Adate et al. \(1996\)](#). Clay samples were analysed after ethylene-glycol saturation. The
151 kaolinite/(illite+chlorite) ratios ($K/(I+C)$) were calculated to trace the relationship between
152 chemical and physical alteration (e.g., [Duchamp-Alphonse et al., 2011](#)). High $K/(I+C)$ values
153 suggest high chemical alteration related to more hydrolysing conditions under a warm and
154 humid climate. The detrital index (DI) was calculated by dividing the sum of detrital minerals
155 (quartz, phyllosilicates, Na-plagioclase, K-feldspar) by the calcite content (e.g., [Adate et al.,](#)
156 [2002](#)). High DI values indicate high input of terrigenous material and/or decreased carbonate
157 production/ increased dissolution.

158

159 3.2. *Elemental geochemistry*

160 Major (MEs; Si, Ti, Al, Ca, Na) and trace (TEs; Cu, Ni, Co, Cr, V, U, Mo, Zr)
161 elements concentrations were determined by X-ray fluorescence spectrometry (XRFS), using
162 a PANalytical PW2400 spectrometer. MEs were determined on fused lithium tetraborate glass
163 disks, and TEs on pressed pellets of powdered whole-rock samples mixed with Mowiol
164 polyvinyl alcohol (2%). Analytical reproducibility monitored by replicate analyses of selected
165 samples was lower than $\pm 5\%$ for MEs and TEs. Analysis accuracy was assessed using
166 international and in-house standard reference materials (TS1-Cement, TS3-Clay, TS4-
167 Limestone, TS5-Marlstone, TS7-Sandstone, 372-Portland cement, 368-Dolomite).

168 A chemical index of alteration (CIA*), corrected for the carbonate content (McLennan
169 et al., 1993; Fedo et al., 1995), was used to estimate the intensity of alteration related to
170 paleoclimatic conditions (Nesbitt and Young, 1989).

171
$$\text{CIA}^* = [\text{Al}_2\text{O}_3 / (\text{Al}_2\text{O}_3 + \text{Na}_2\text{O} + \text{CaO}^* + \text{K}_2\text{O})] * 100$$

172 MEs and TEs were Al-normalised to correct for the dilution effect caused by variable
173 proportions of the detrital mineral phases such as aluminosilicates that are of low mobility
174 during diagenetic processes (Tribovillard et al., 2006). Al-normalisation is generally used
175 when the coefficient of variation of Al concentration is not larger than that of other MEs and
176 TEs (Riquier et al., 2006; Tribovillard et al., 2006). The detrital fluxes was evaluated based on
177 Ti, Zr, and Si, and the oxygenation conditions with redox-sensitive TEs such as U, Mo, V, Ni
178 and Cu.

179 Enrichment factors $\text{EF}_{\text{element}(X)} = (\text{X}/\text{Al})_{\text{sample}} / (\text{X}/\text{Al})_{\text{average shale}}$ (Brumsack et al., 2006;
180 Tribovillard et al., 2006) were calculated to evaluate the relative enrichment of the element
181 (X) compared to the average shale composition (Wedepohl, 1971). $\text{EF} > 3$ represents a

182 detectable authigenic enrichment of an element over average shale concentrations, whereas
183 $EF > 10$ represents a moderate to strong degree of authigenic enrichment (e.g., [Tribovillard et](#)
184 [al., 2006](#); [Algeo and Tribovillard, 2009](#)).

185

186 *3.3. Phosphorus*

187 To extract total phosphorus (P_{tot}), 1 mL of 1M $Mg(NO_3)_2$ was added to 100 ± 5 mg of
188 powdered whole-rock sample and then placed in an oven at $550^\circ C$ during 2h30. After cooling
189 10 mL of HCl (1N) was added. The preparation was then placed on a shaker for 16h in order
190 to liberate the P_{tot} . Samples were then filtered ($0.45 \mu m$) and analysed using the ascorbic acid
191 method ([Eaton et al., 1995](#)). In addition, the SEDEX sequential extraction method developed
192 by [Ruttenberg \(1992\)](#) and adapted by [Mort et al. \(2007\)](#) was used to quantify the authigenic
193 (P_{auth}), detrital (P_{det}) and organic (P_{org}) P phases. P concentrations (ppm) were measured using
194 an UV/Vis Perkin Elmer Spectrophotometer. C_{org}/P_{org} and C_{org}/P_{tot} (Redfield) molar ratios were
195 calculated (C_{org} = total organic carbon).

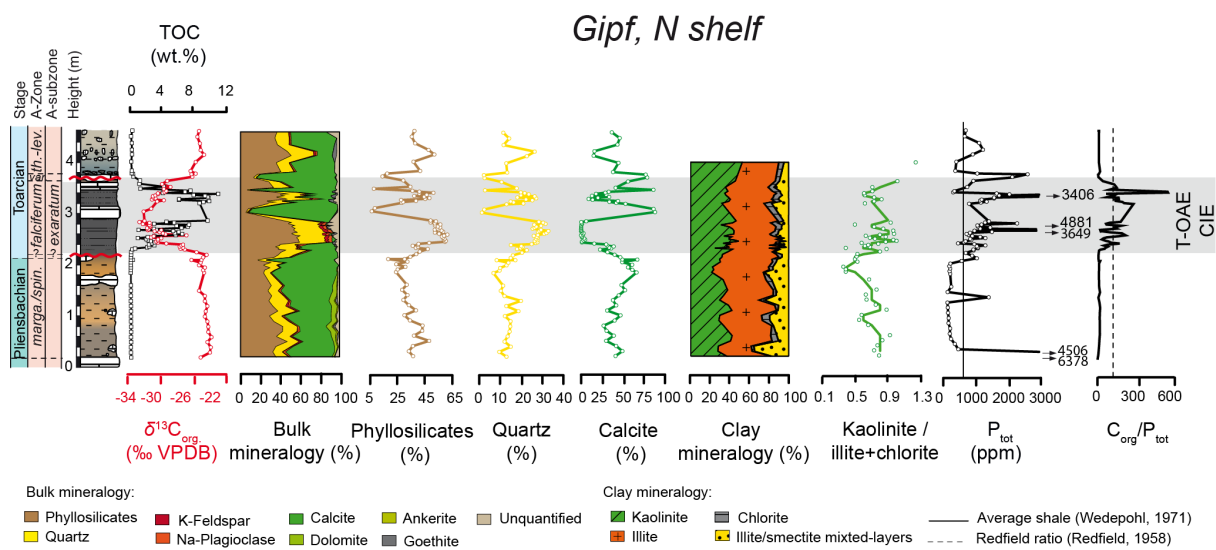
196

197 **4. Results**

198 *4.1. Whole-rock mineralogy and clay mineralogy*

199 At Gipf, phyllosilicates (17-61%), calcite (3-77%) and quartz (2-26%) are the
200 dominant minerals in the clayey marl and marl, whereas calcite (78-88%) dominates the
201 limestone beds ([Fig. 3](#)). Phyllosilicates and quartz show a decreasing trend towards the
202 Pliensbachian-Toarcian boundary followed by an abrupt increase at the base of the CIE
203 interval, which coincides with a drop in calcite content to 0.3%. The presence of goethite
204 throughout the section is likely related to the oxidation of pyrite ([Nordstrom, 1982](#)). Clay-

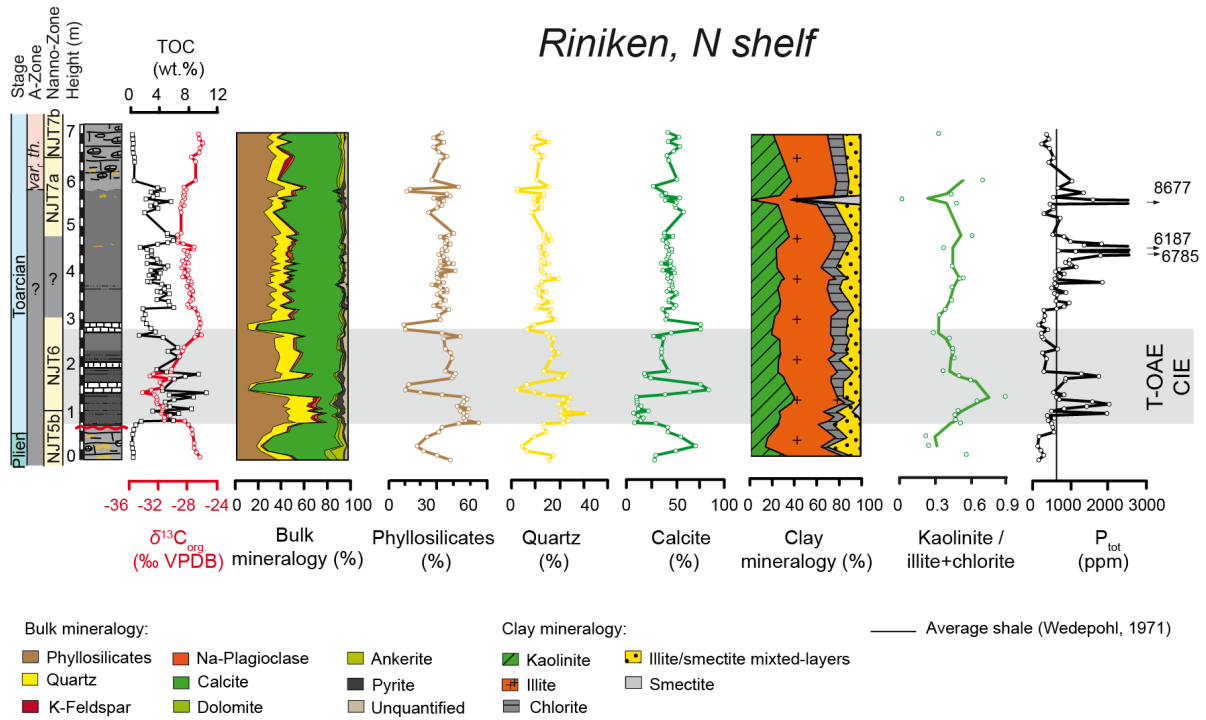
205 mineral assemblages consist mainly of kaolinite (21-52%), illite (34-58%), chlorite (1-11%)
 206 and illite/smectite mixed-layers (2-35%) (Fig. 3). Kaolinite and K/(I+C) show a decrease
 207 towards the Pliensbachian-Toarcian boundary. This is followed by a marked increase in
 208 kaolinite (up to 49%) and K/(I+C) at the onset of the negative CIE. Then, a transient decrease
 209 is observed in the upper portion of the negative CIE interval below a second increase in the
 210 *thouarsense-levesquei* zones (Upper Toarcian) (Fig. 3).



211
 212 **Fig. 3.** Stratigraphic variations in the total organic carbon (TOC) content, organic-carbon isotopes ($\delta^{13}C_{org}$), whole-rock and
 213 clay mineralogy, total phosphorus (P_{tot}) content, and C_{org}/P_{tot} ratios along the Gipf section (northern shelf).

214
 215 At Riniken, phyllosilicates (18-55%), calcite (8-70%), quartz (4-31%) dominate the
 216 whole-rock composition in the clayey and marly intervals, whereas calcite is the dominant
 217 mineral (64-83%) in the limestone beds. Phyllosilicates and quartz show a decrease towards
 218 the Pliensbachian-Toarcian boundary interval, whereas calcite increases. A sharp decrease in
 219 the calcite content to 8% is observed at the base of the CIE interval, whereas phyllosilicates
 220 and quartz increase (up to 55% and 31%, respectively). The clay fraction is mainly composed
 221 of kaolinite (13-40%), illite (33-62%), chlorite (3-19%) and illite/smectite mixed-layers (5-
 222 31%) (Fig. 4). Smectite is present in low amounts at the base of the section (at 0.90m: 2% and
 223 at 1.05m: 8%). A peak in smectite is observed at 5.6 m (56%) and corresponds to a

224 lithological change. A marked increase in kaolinite and K/(I+C) is observed at the base of the
 225 CIE interval, followed by a decrease in the upper portion of this interval and a long-term
 226 increasing trend section upward (Fig. 4).



227

228 **Fig. 4.** Stratigraphic variations in the total organic carbon (TOC) content, organic-carbon isotopes ($\delta^{13}\text{C}_{\text{org}}$), whole-rock
 229 mineralogy, clay-mineral assemblages, and total phosphorus (P_{tot}) content at Riniken (northern shelf).

230

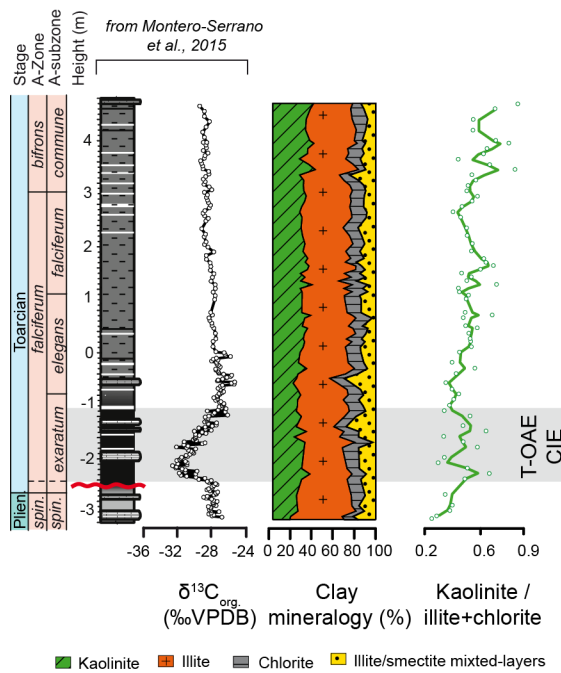
231 At Rietheim, the clay fraction is dominated by kaolinite (16-41%), illite (29-56%),

232 chlorite (5-24%) and illite/smectite mixed-layers (3-34%) (Fig. 5). Kaolinite and K/(I+C)

233 increase at the base of the CIE interval. A transient decrease in kaolinite is observed in the

234 upper portion of the CIE, followed by a long-term increase up to the top of section.

Rietheim, N shelf



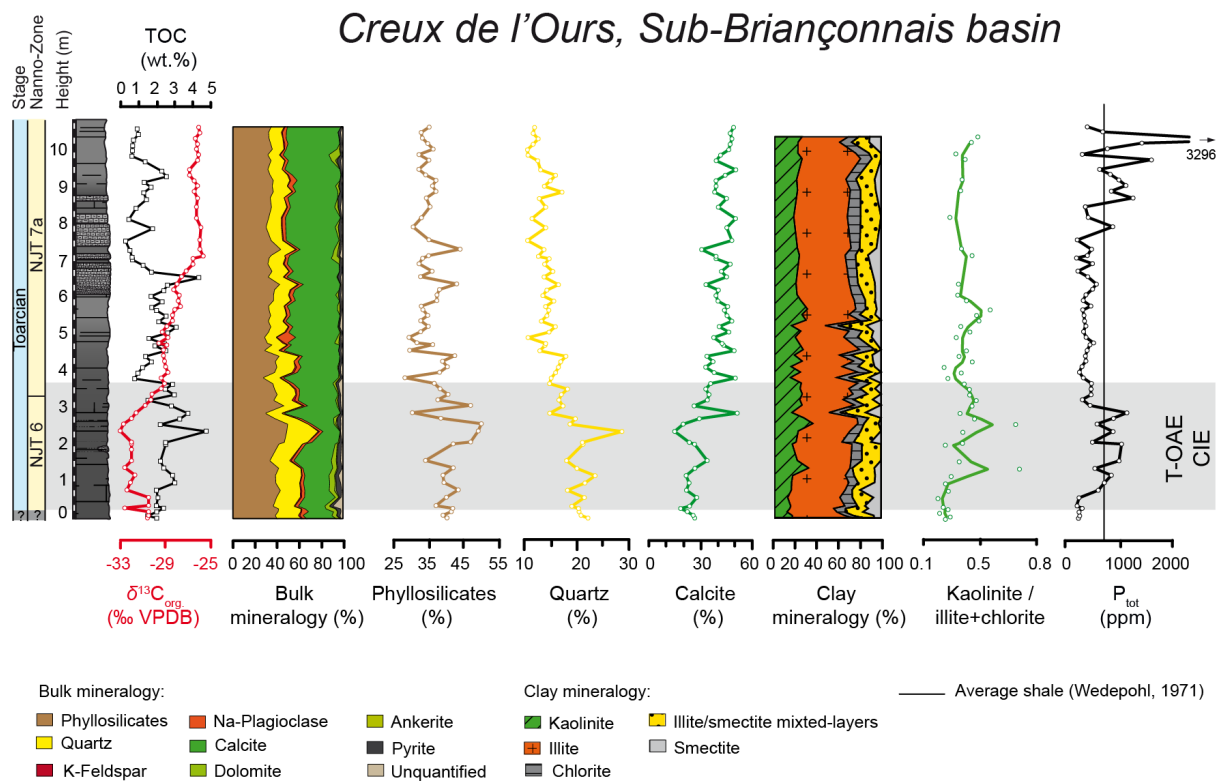
235

236 **Fig. 5.** Clay-mineral distribution and organic-carbon isotopes ($\delta^{13}\text{C}_{\text{org}}$) at Rietheim (northern shelf).

237

238

At Creux de l'Ours, the Lower Toarcian marl mainly consists of calcite (15-51%),
 239 phyllosilicates (28-50%) and quartz (10-29%), with lower proportions of K-feldspar, Na-
 240 plagioclase, dolomite and ankerite (Fig. 6). The calcite content shows the lowest values within
 241 the CIE interval (mean is 27%) and then gradually increases section upward. This is inversely
 242 correlated with phyllosilicates and quartz, both having the highest values within the CIE
 243 interval (up to 50% and up to 49%, respectively). The clay-mineral assemblage consists
 244 predominantly of illite (30-56%) and kaolinite (12-36%), and in lower proportions of chlorite
 245 (2-15%), smectite (0-19%) and illite/smectite mixed-layers (6-26%) (Fig. 6). The negative
 246 CIE is marked by an increase in kaolinite (from 16% to 35%) and K/(I+C). This is followed
 247 by a decrease in the upper portion of the CIE and a long-term increase section upward.



248

249 **Fig. 6.** Stratigraphic variations in the total organic carbon (TOC) content, organic-carbon isotopes ($\delta^{13}C_{org}$), whole-rock
 250 mineralogy, clay-mineral assemblages, and total phosphorus (P_{tot}) content at Creux de l'Ours (Sub-Briançonnais basin).

251

252

253

254

255

256

257

258

259

260

261

At Breggia, the Pliensbachian-Toarcian interval is dominated by calcite (40-86%),

phyllosilicates (5-34%) and quartz (3-20%) (Fig. 7). Calcite is inversely correlated with

phyllosilicates and quartz. Quartz and phyllosilicates increase just above the stratigraphic gap

(*tenuicostatum-falciferum* zones). This is followed by a transient decrease and a long-term

increase from the uppermost part of the CIE (from 1.6 m) section upward. The clay fraction is

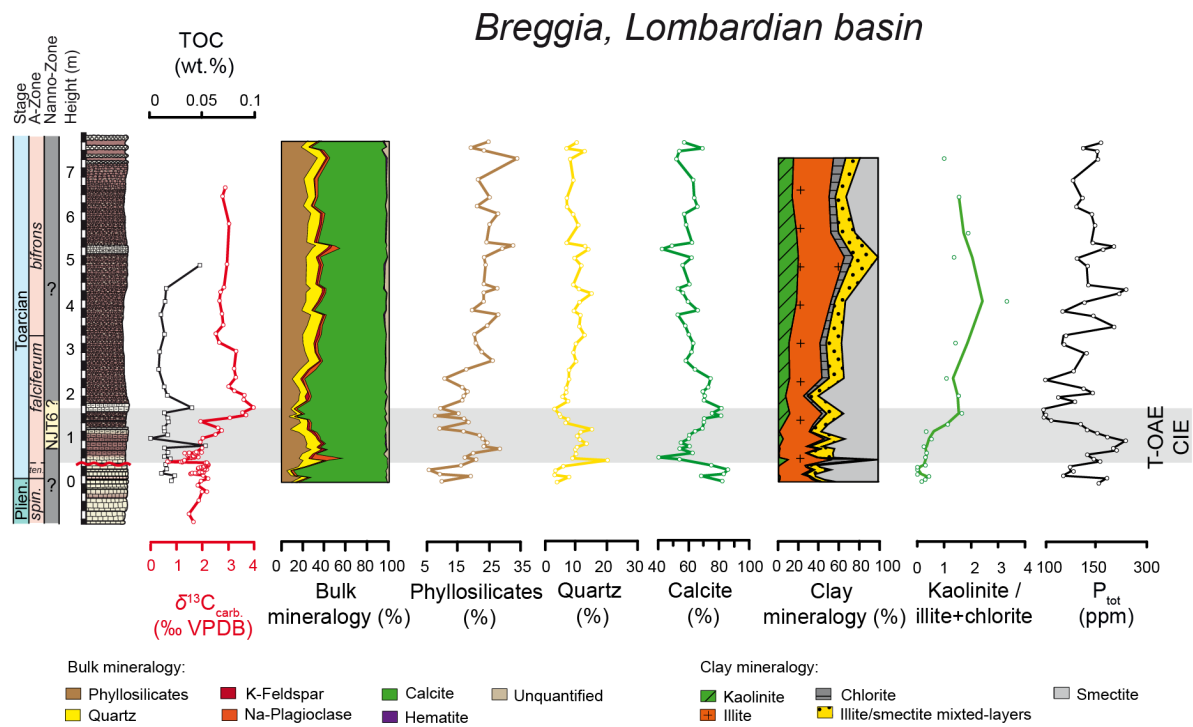
dominated by illite and smectite, with lower proportions of chlorite, kaolinite and

illite/smectite mixed-layers. Smectite and illite dominate the assemblage (up to 60 and 45%,

respectively) in the CIE interval, whereas kaolinite is nearly absent (0-2%). The K/(I+C) ratio

is low and increases in the upper portion of the CIE and onwards, together with kaolinite (up

to 20%) (Fig. 7).



262

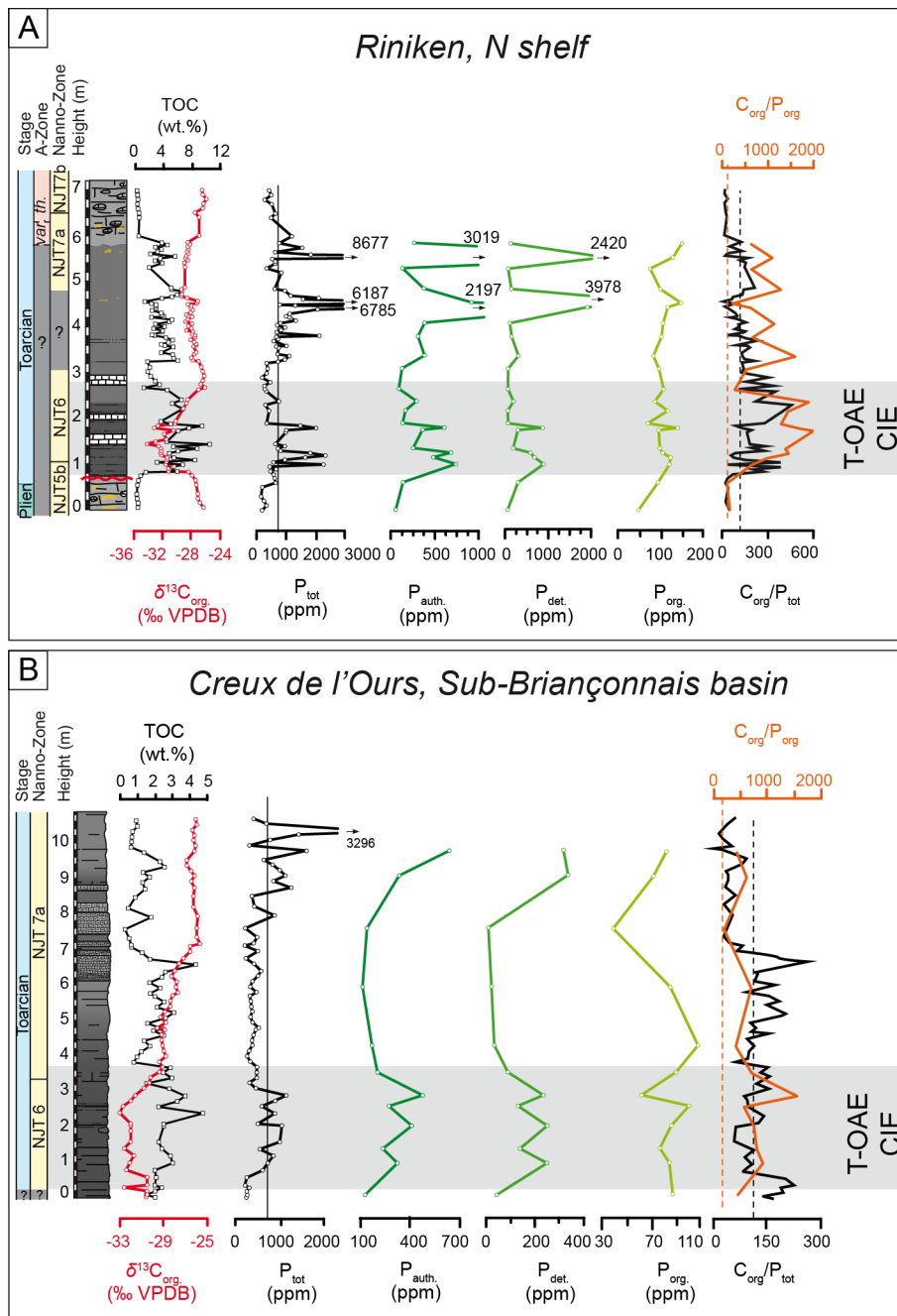
263 **Fig. 7.** Stratigraphic variations in the total organic carbon (TOC) content, organic-carbon isotopes ($\delta^{13}\text{C}_{\text{org}}$), whole-rock and
 264 clay mineralogy, and the total phosphorus (P_{tot}) content along the Breggia section (Lombardian basin).

265

266 *4.3. Phosphorus*

267 At Gipf, P_{tot} content is low (150-480 ppm) in the Upper Pliensbachian interval except
 268 for two peaks of >1000 ppm (Fig. 3). The CIE interval is marked two main P_{tot} increases (up
 269 to 4880 ppm and 3406 ppm, respectively) and high $\text{C}_{\text{org}}/\text{P}_{\text{tot}}$ ratios (up to 540 ppm). This is
 270 followed by a return to background concentrations in the upper portion of the CIE interval
 271 (mean: 308 ppm) and a sharp increase to 2600 ppm in the condensed limestone bed at 3.7 m
 272 (Fig. 3).

273 At Riniken, P_{tot} increases up to 2370 ppm at the base of the CIE interval (Figs. 4 and
 274 8), followed by a decrease (180-760 ppm) in the upper part of this interval. Two intervals of
 275 very high values (up to 6785 and 8677 ppm, respectively) are observed in the upper part of
 276 the section and correspond to phosphatic crusts and concretions in the marly limestone.



277 --- C_{org}/P_{org} (Redfield, 1958) --- C_{org}/P_{tot} (Redfield, 1958) — Average shale value (Wedepohl, 1971)

278 **Fig. 8.** Phosphorus speciation ($P_{det.}$, $P_{auth.}$, $P_{org.}$) at (A) Riniken and (B) Creux de l'Ours, plotted against the organic-carbon
 279 isotopes ($\delta^{13}C_{org}$) and the total organic carbon (TOC) content.

280

281 The main P phases are $P_{auth.}$ (mean: 520 ppm), and $P_{det.}$ (mean: 633 ppm), whereas $P_{org.}$

282 shows lower values (mean: 106 ppm) (Fig. 8A). $P_{auth.}$ and $P_{det.}$ show trends similar to P_{tot} ($r^2 =$

283 0.88 and 0.80, respectively). $P_{org.}$ increases at the onset of the CIE interval and then remains

284 relatively constant section upward. The C_{org}/P_{tot} and C_{org}/P_{org} ratios show parallel trends and
285 reach maximum values in the CIE interval (449 and 2000, respectively) (Fig. 8A).

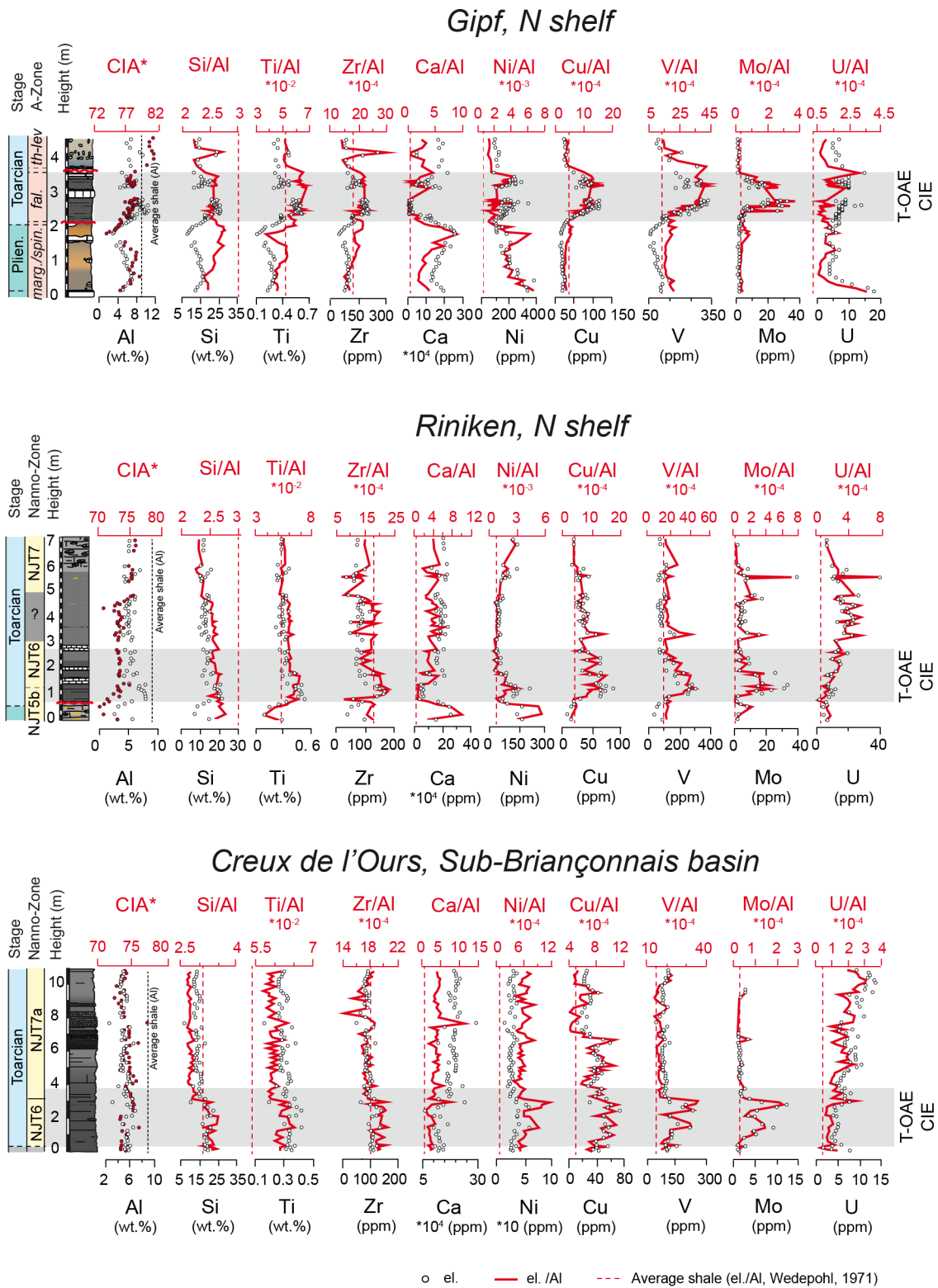
286 At Creux de l'Ours, the base of the CIE interval shows an increase in P_{tot} values (up to
287 1150 ppm), followed by a return to background values (236-474 ppm) in the upper part of this
288 interval (Figs. 6 and 8B). Maximal values (3296 ppm) are reached in the upper part of the
289 section. P_{auth} (mean: 283) and P_{det} (mean: 154 ppm) are the main P phases and follow P_{tot}
290 distribution (Fig. 8B). P_{org} is a minor phase (mean: 82 ppm) and shows higher values across
291 the CIE interval, followed by generally lower values above this interval. C_{org}/P_{tot} ratios are low
292 and show constant values (mean: 127) within the CIE interval. The C_{org}/P_{org} ratio shows higher
293 values than C_{org}/P_{tot} and maximal values (1550) are reached in the CIE interval (Fig. 8B).

294 At Breggia, P_{tot} values are low (100-260 ppm) and show a slight increase (up to 260
295 ppm) within the CIE interval (Fig. 7). This is followed by a decrease in the upper portion of
296 this interval and a long-term increasing trend section upward.

297

298 4.4. Major and trace element abundances

299 At Gipf, Si, Ti, and Zr show a good correlation with Al ($r^2 = 0.97, 0.91, 0.90$,
300 respectively) and exhibit trends similar to the CIA* (Fig. 9). They all show a sharp increase
301 just below the Pliensbachian-Toarcian boundary and maximum values in the CIE interval,
302 followed by a return to background values. Ti/Al and Zr/Al display their highest values in the
303 CIE interval, whereas Si/Al shows relatively stable values along the section (Fig. 9). Cu/Al,
304 V/Al and Mo/Al show the highest values in the CIE interval, followed by a return to
305 background values (Fig. 9).



306

307
308
309

Fig. 9. Stratigraphic evolution of major and trace elements for the sections of Gipf, Riniken and Creux de l'Ours. The CIA* values are plotted against the Al trend. The data are shown in absolute (wt.% and ppm; black dots) and Al-normalised (red lines) contents.

310 Ni/Al and U/Al show a decreasing trend below the Pliensbachian-Toarcian boundary,
311 followed by a slight increase at the onset of the CIE and then a return to lower values after
312 this interval (Fig. 9).

313 At Riniken, Si, Ti, and Zr are moderately correlated with Al ($r^2= 0.96, 0.93, 0.59$).
314 Ti/Al, Zr/Al and CIA* reach maximum values at the base of the CIE interval (Fig. 9). Si/Al
315 shows the highest values below the Pliensbachian-Toarcian boundary and then a decreasing
316 trend section upward. Cu/Al, V/Al and Mo/Al reach maximum values at the base of the CIE
317 interval (Fig. 9). Ni/Al shows the highest values in the Upper Pliensbachian interval and a
318 sharp decrease just below the CIE interval. A slight increase is observed at the base of the
319 CIE, followed by a return to lower values section upward. U/Al shows a gradual increase
320 from the base to the top of the section, reaching its maximum value above the CIE interval.

321 At Creux de l'Ours, Si, Ti, and Zr are highly correlated with Al ($r^2=0.78, 0.96, 0.87$,
322 respectively) and display a trend similar to the CIA*. Si/Al, Ti/Al, Zr/Al and CIA* show the
323 highest values within the CIE interval and a decreasing trend section upward (Fig. 9). Ni/Al,
324 Cu/Al, V/Al, Mo/Al and U/Al show the highest values within the CIE interval. Ni/Al, V/Al
325 and Mo/Al display a sharp decrease in the second part of the CIE interval, whereas Cu/Al
326 exhibit more fluctuating values. U/Al shows an increase from the base to the top of the
327 section (Fig. 9).

328

329 **5. Discussion**

330 *5.1. Clay minerals*

331 *5.1.1. Preservation of the primary clay minerals*

332 The late diagenetic effect on the primary clay mineral assemblage must be evaluated
333 before any paleoenvironmental interpretation (e.g., Chamley, 1989; Kübler and Jaboyedoff,
334 2000). At Gipf, Riniken and Rietheim (northern shelf), T_{max} values up to 440°C and the
335 absence of smectite suggest a moderate diagenetic overprint, because smectite commonly
336 transforms into illite when burial depth reaches about 2000 m and/or when T_{max} values reach
337 430-440°C (Burtner and Warner, 1986; Chamley, 1989). In these successions, burial depth
338 may have been underestimated and the geothermal gradient higher due to the proximity to the
339 Rhine graben (Todorov et al., 1993). At Creux de l'Ours (Sub-Briançonnais basin) and
340 Breggia (Lombardian basin), the presence of smectite and the low abundance of illite/smectite
341 mixed-layers indicate a weak diagenetic overprint and/or neoformation of smectite. Indeed,
342 the presence of radiolarians in these more open-marine sections may have been a source of
343 dissolved Si, which was subsequently involved in the precipitation of authigenic smectite
344 (Chamley, 1989). The weak influence of burial diagenesis is supported by T_{max} values up to
345 435°C and 439°C, respectively (Deconinck and Bernoulli, 1991; Fantasia et al., in review).

346 In all studied sections, the presence of kaolinite suggests that the diagenetic overprint
347 was however not too strong and variations in the clay-mineral assemblages likely reflect a
348 primary paleoenvironmental signal. K/(I+C) ratios combined with CIA* values were used to
349 trace changes in hydrolysing conditions and humidity variations.

350

351 *5.1.2. Paleoclimatic conditions*

352 At Gipf, Riniken, Rietheim (northern shelf) and Creux de l'Ours (Sub-Briançonnais
353 basin), K/(I+C) ratios display comparable trends (Fig. 10). The low K/(I+C) ratios in the
354 Upper Pliensbachian intervals may indicate a relatively cool to temperate and/or dry climate
355 (Chamley, 1989; Velde, 1995). This is supported by the relatively low CIA* values compared

356 to the Toarcian interval. The Late Pliensbachian was marked by a regression (Haq et al.,
357 1987; Hardenbol et al., 1998; Haq, 2017), which supports the interpretation that the decrease
358 in kaolinite is likely related to paleoclimatic conditions rather than to sea-level change. The
359 increase of K/(I+C) and CIA* values at the onset of the CIE, suggests a shift towards a
360 warmer and more humid climate (Thiry, 2000), which led to increased hydrolysing conditions
361 on the surrounding landmasses during the T-OAE (Fig. 10). This major change in the clay-
362 mineral assemblage was also observed in other NW European basins (Dera et al., 2009;
363 Hermoso and Pellenard, 2014; Bougeault et al., 2017).

364 The distal paleogeographic position of the sections of Creux de l'Ours (Sub-
365 Briançonnais basin) and Breggia (Lombardian basin) (Thierry, 2000) coupled with the Early
366 Toarcian transgression (Haq et al., 2017), likely interfered with the distribution of larger
367 kaolinite clay (e.g., Gibbs, 1977; Adatte et al., 2002; Godet et al., 2008). This could explain
368 lower kaolinite contents in the deepest and more distal settings. In addition, at Breggia, a drier
369 belt along the southern Tethyan margin during the T-OAE (van de Schootbrugge et al., 2005)
370 may have been responsible for the low K/(I+C) ratios owing to low hydrolysing conditions.
371 The predominance of smectite in the CIE interval most likely reflects the weathering of soils
372 developed on a distant landmass under a semi-arid climate with alternating humid and dry
373 seasons (Singer, 1984; Chamley, 1989). The high content in illite suggests a nearby clastic
374 source; such may have been the Gozzano High, located to the west of the Lombardian basin,
375 and uplifted during the latest Triassic-Early Jurassic (Bernoulli and Ulmer, 2016). Deconinck
376 and Bernoulli (1991) assigned the diversity of the clay-mineral assemblages at Breggia to the
377 weathering of various parent materials, including soils and crystalline basement. Above the
378 CIE interval, the gradual increase in kaolinite relative to smectite is likely related to a shift
379 towards warmer and more humid conditions rather than to sea-level rise, which would have
380 rather lead to an increase in smectite contents (Figs. 7 and 10). This trend is similarly

381 observed in the other studied sections and coincides with high CIA* values. Therefore, the
382 hydrolysing conditions, induced by the warm and humid climate initiated during the Early
383 Toarcian, appear to have prevailed well after the CIE interval in the Alpine Tethys (up to the
384 *bifrons* Zone; [Dera et al., 2009](#)).

385

386 5.2. Change in continental weathering

387 At Gipf, Riniken (northern shelf) and Creux de l'Ours (Sub-Briançonnais basin), the
388 CIE interval is marked by an increase (or the highest values) in the CIA*, detrital index and
389 detrital elements ([Figs. 9 and 10](#)). This suggests that the climate shift towards warmer and
390 more humid climate (high kaolinite) increased the weathering rate in the nearby source areas
391 during the T-OAE. The increase in the detrital index is thus likely related to (i) the increase in
392 continental runoff, (ii) significant reworking during the early transgressive phase, (iii) a
393 decrease in the calcite content (acidification) due to the injection of greenhouse gases into the
394 atmosphere and the ocean (e.g., [Suan et al., 2008](#); [Trecalli et al., 2012](#)). High Ti/Al and Zr/Al
395 during the CIE may be related to enhanced detrital supply from fluvial discharge, since these
396 elements are generally associated with heavy mineral grains (ilmenite, rutile, zircon) and/or to
397 an increase in eolian supply ([Riquier et al., 2006](#)). Ti and Zr might also have been enriched
398 relative to more labile elements due to the stronger hydrolysing conditions. These results are
399 in good agreement with other studies from the European areas (e.g., [Cohen et al., 2004](#);
400 [Hermoso and Pellenard et al., 2014](#); [Brazier et al., 2015](#)). Higher hydrolysing conditions
401 favoured higher nutrient fluxes into the basins, ultimately boosting primary productivity and
402 the development of oxygen-depleted conditions ([Jenkyns, 2010](#)). It is not excluded that the
403 deep and more distal setting of the Creux de l'Ours section modulated detrital input and
404 nutrient fluxes.

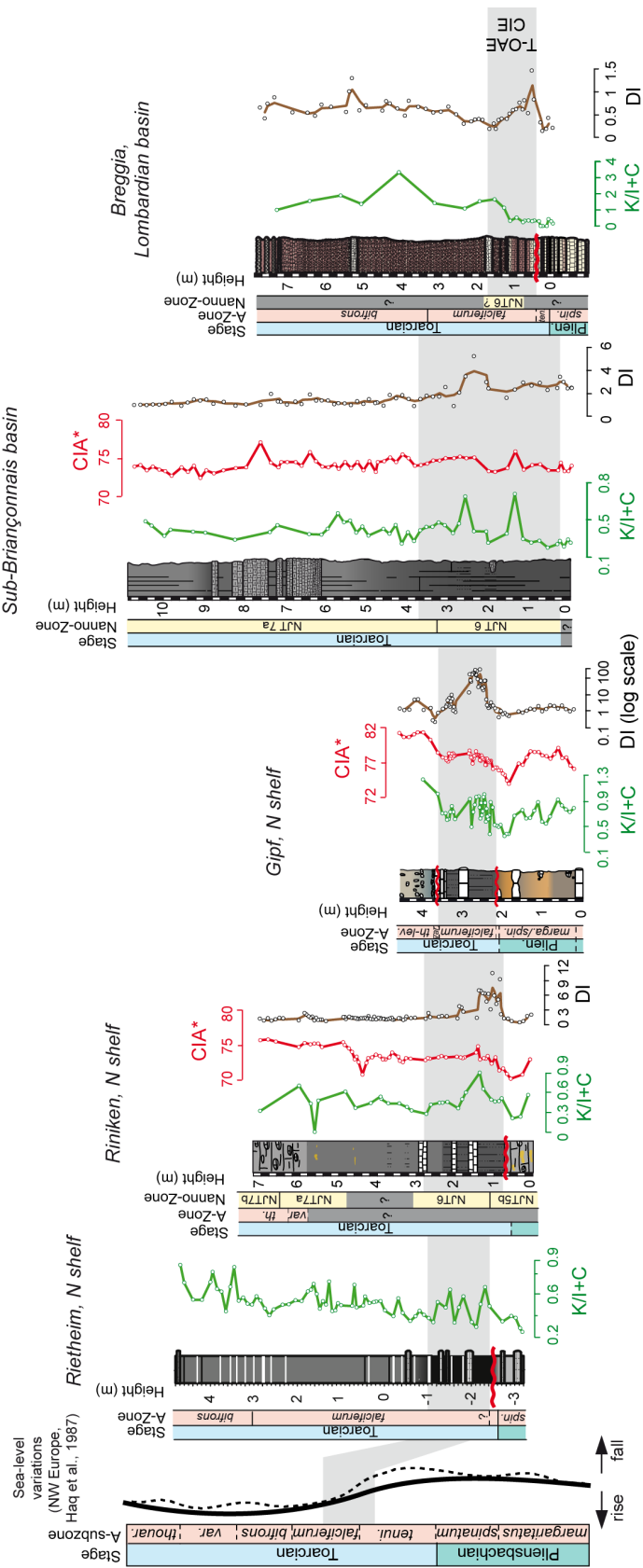


Fig. 10. Evolution of the kaolinite/illite+chlorite (K/(I+C)) ratios, the chemical index of alteration (CIA*) and the detrital index (DI) along the studied transect, plotted against the sea-level curve for NW Europe (Haq et al., 1987). The CIE interval records a general increase in terrigenous input (increase in DI values) linked with higher hydrolysing conditions (higher kaolinite content and higher CIA* values).

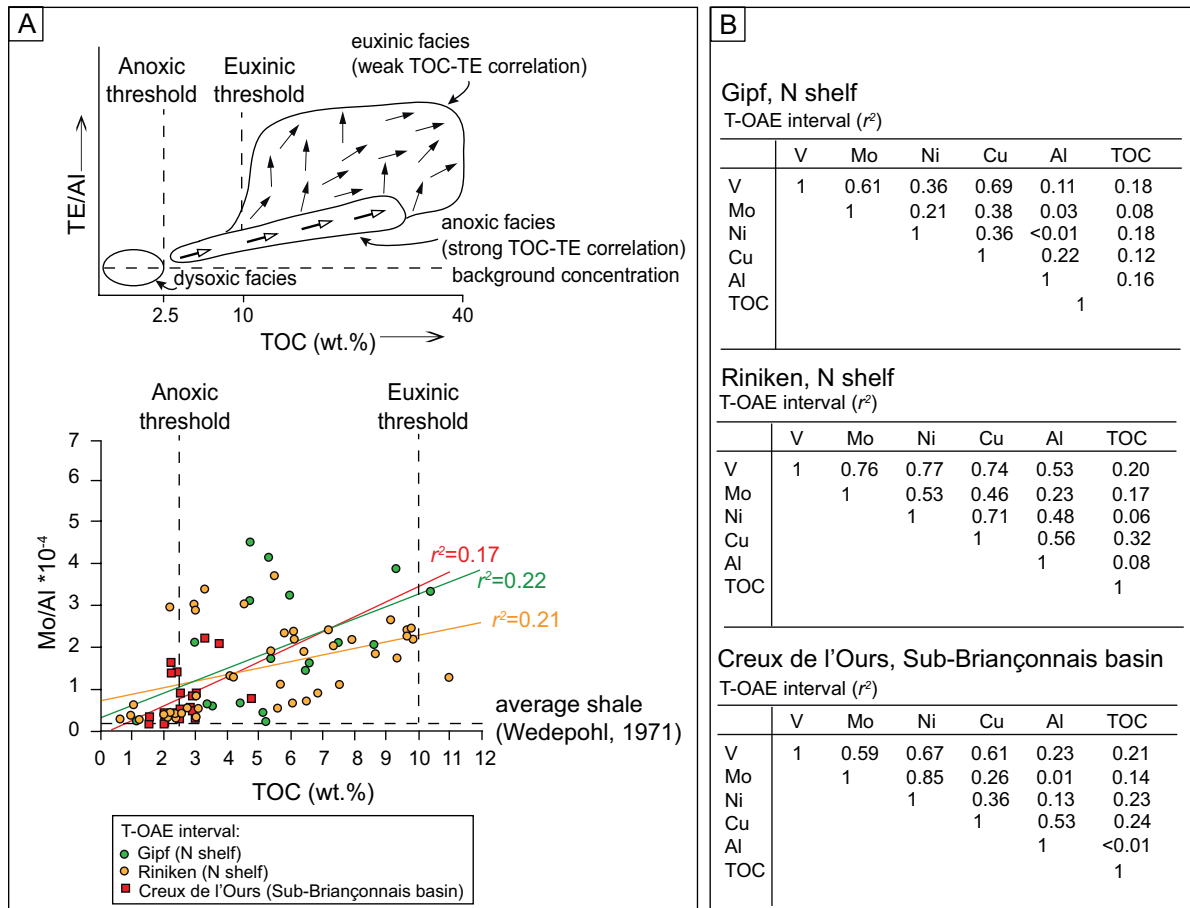
410 At Breggia (Lombardian basin), the low hydrolysing conditions (low kaolinite)
411 recorded in the upper part of CIE coupled with the deeper and more distal setting likely
412 limited detrital input. The slight increase in the detrital index in this interval is rather linked to
413 condensation (distal setting and carbonate dissolution) rather than to higher detrital input.
414 Indeed, the T-OAE was marked by a general biocalcification crisis in pelagic and benthic
415 communities, which was attributed to eutrophication and changes in ocean chemistry (e.g.,
416 [Mattioli et al., 2008](#); [Trecalli et al., 2012](#); [Reolid et al., 2014](#); [Ferreira et al., 2017](#)). This led to
417 the near disappearance of shallow-water platforms and the decrease in carbonate
418 accumulation in the deepest parts of the basins ([Blomeier and Reijmer, 1999](#); [Mattioli et al.,](#)
419 [2008](#); [Trecalli et al., 2012](#)). Therefore, condensation related to the decrease in carbonate
420 production might have been more important in carbonate-dominated settings like at Breggia.

421

422 *5.3. Redox conditions*

423 At Gipf, Riniken (northern shelf) and Creux de l'Ours (Sub-Briançonnais basin), the
424 increasing trends in redox-sensitive TEs (V, Mo, Cu, Ni) coupled with low to modest EFs
425 (Gipf: 1-13; Riniken: 0.5-21; Creux de l'Ours: 0.6-12) during the T-OAE interval indicate a
426 shift towards oxygen-depleted conditions ([Figs. 9 and 12A](#)). These elements tend to be less
427 soluble under reducing conditions, and depend on the flux of OM delivered to the sediments
428 and the formation of sulphides (mainly pyrite), whose accumulation is largely controlled by
429 the oxygenation conditions of the sedimentary environment ([Riquier et al., 2006](#); [Tribovillard](#)
430 [et al., 2006](#); [Calvert and Pederson, 2007](#)). The Mo-TOC scatterplot indicate that sediments
431 were deposited under dysoxic to anoxic conditions at Gipf and Riniken and mostly under
432 dysoxic conditions at Creux de l'Ours in the T-OAE interval ([Fig. 11A](#)). This is supported by
433 the absence of genuine laminated organic-rich sediments in the latter. In addition,

434 sedimentological features (e.g., obliquely-bedded laminae and homogeneous mud layers
 435 containing rip-up clasts) observed in these successions (Fantasia et al., in review) indicate that
 436 short episodes of winnowing and sediment reworking likely precluded the development of
 437 strong and persistent bottom-water anoxia in these sections.



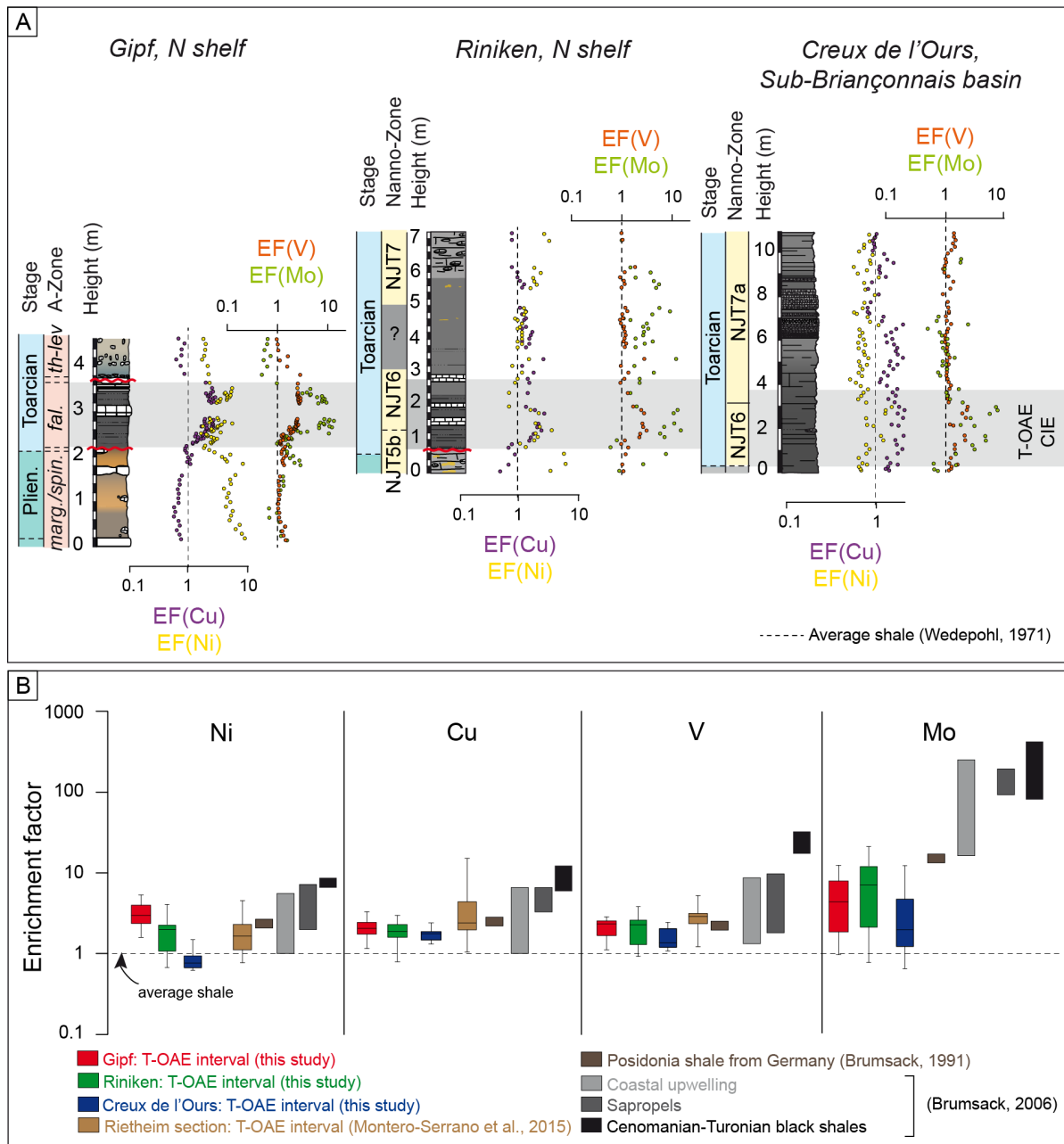
438

439 **Fig. 11.** (A) Comparative Mo-TOC scatterplots for the T-OAE interval from Gipf, Riniken and Creux de l'Ours, according to
 440 Algeo and Maynard (2004). Square linear regressions are shown for the three sections. (B) Correlation factors (r^2) of selected
 441 trace elements measured in the T-OAE interval at Gipf, Riniken and Creux de l'Ours.

442

443 The poor correlation of Ni, Cu, V and Mo with TOC and Al indicates that these
 444 elements were mainly enriched through redox processes (Fig. 11B). EFs of V, Mo, Ni and Cu
 445 are lower than the EFs from sites characterised by strong anoxia (e.g., Brumsack, 2006),
 446 supporting our interpretation that dysoxic to anoxic conditions developed during the T-OAE
 447 interval rather than strong anoxia or euxinia (Fig. 12B). At Gipf, Riniken and Creux de

448 l'Ours, U shows a trend different to the other redox-sensitive TEs, especially above the CIE
 449 interval. This may be due to variability in the sedimentation-accumulation rate (Wignall and
 450 Maynard, 1993) and/or to adsorption onto authigenic phosphate (Abed et al., 2013).



451

452 **Fig. 12.** (A) Evolution of the enrichment factors (EFs) for trace elements (Ni, Cu, V, Mo) measured at Gipf, Riniken and
 453 Creux de l'Ours, relative to average shale (Wedepohl, 1971). (B) Enrichment factors (EFs) for Ni, Cu, V and Mo from the T-
 454 OAE interval of the studied sections of Gipf, Riniken and Creux de l'Ours compared with other organic-rich sections
 455 (Brumsack, 1991, 2006; Montero-Serrano et al., 2015).

456

457 At Gipf, Riniken and Creux de l'Ours, Ni/Al and Cu/Al show a slight to sharp increase
458 in the T-OAE interval, which coincides with an interval of high OM content (Fig. 9). These
459 elements are generally delivered and retained in the sediment in association with OM under
460 reducing conditions (Algeo and Maynard, 2004; Tribovillard et al., 2006). Therefore, the
461 increase in Ni and Cu within the T-OAE likely indicates a higher OM flux and thus
462 potentially higher productivity. High Ni concentrations appear to be coupled with high Ca
463 values in the marly limestone from the Pliensbachian and Upper Toarcian, likely due to the
464 preferential precipitation of Ni in carbonate complex (Tribovillard et al., 2006).

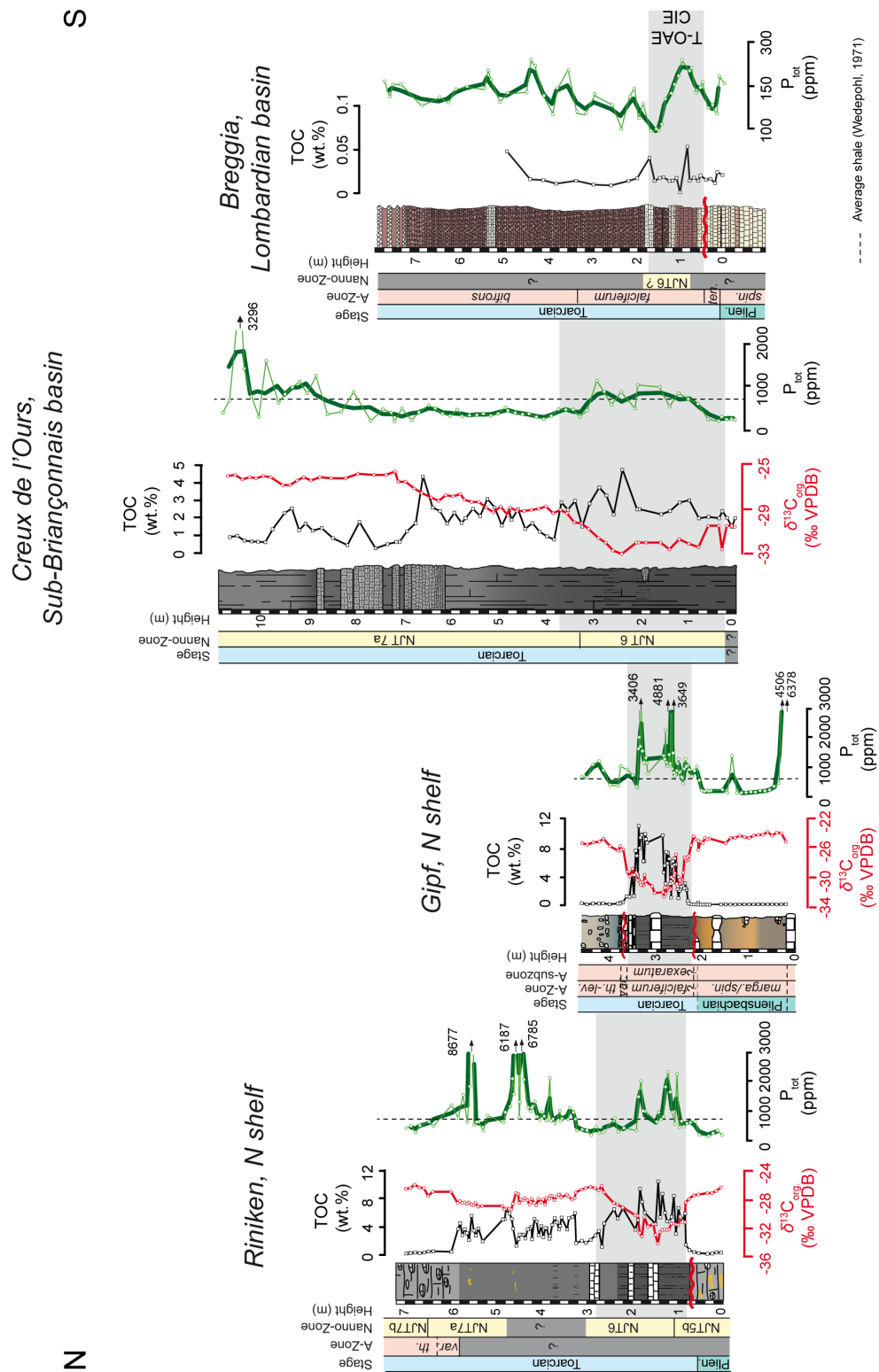
465 At Breggia (Lombardian basin), the degree of oxygenation is inferred from
466 sedimentological observations. Even if the lower part of the negative CIE is missing due to a
467 stratigraphic gap, the presence of abundant bioturbation and the absence of OM in the interval
468 showing the return to more positive values in the CIE indicate that oxic conditions prevailed
469 (Fantasia et al., in review).

470

471 *5.4. Insights from phosphorus*

472 At Gipf, Riniken (northern shelf) and Creux de l'Ours (Sub-Briançonnais basin), high
473 P_{tot} values coupled with high TOC values are recorded in sediments deposited under dysoxic
474 to intermittently anoxic conditions (Fig. 13). Mesozoic OAEs generally show a drastic
475 decrease in P_{tot} because P is strongly dependent on redox conditions at the sediment-water
476 interface and generally released to the water column under reducing conditions (e.g., Van
477 Cappellen and Ingall, 1994; Föllmi, 1996; Mort et al., 2007). Consequently, P may increase
478 primary productivity, expand the oxygen-minimum zone and reinforce the sinking flux of
479 organic carbon in a positive feedback loop (van Cappellen and Ingall, 1994; Filippelli and
480 Delaney, 1996; Mort et al., 2007). On the other hand, under oxic conditions, part of the

481 remineralised organic P may be trapped in the sediment mainly through authigenesis and
482 adsorption on clay minerals and Fe-oxyhydroxides ([Slomp et al., 1996](#); [Algeo and Ingall,](#)
483 [2007](#)).



484

485 **Fig. 13.** Variations in phosphorus (P) contents along the studied transect, plotted against the organic-carbon isotopes ($\delta^{13}C_{org}$)
 486 and the total organic-carbon (TOC) content.

487 At Riniken and Creux de l'Ours, C_{org}/P_{org} ratios higher than the Redfield ratio (106:1;

488 Redfield, 1958) in the CIE interval suggests that the retention capacity of P in OM was very

489 low and that preserved OM was depleted in P relative to carbon. P can be laterally transferred
490 into authigenic P during diagenesis and thus C_{org}/P_{org} ratios are commonly used ([Anderson et](#)
491 [al., 2001](#); [Algeo and Ingall, 2007](#)). C_{org}/P_{tot} higher than C_{org}/P_{org} , and both slightly to markedly
492 higher than the Redfield ratio in the CIE interval ([Fig. 8](#)) suggest a lateral transfer of organic-
493 bound P into an authigenic phase and/or the release of P back into the water column. It
494 appears from the thin-sections analysis that the “authigenic” P is mostly related to fish
495 remains (biogenic P), which may have been converted into more stable carbonate fluorapatite
496 ([Schenau and De Lange, 2000](#)). However, P authigenesis cannot be totally excluded. High P_{det}
497 contents observed at Riniken (boundary between NJT6 and NJT7a nanofossil zones) are
498 related to the presence of authigenic P crusts. Indeed, P_{det} may correspond to an authigenic
499 phase, which underwent subsequent recrystallisation (e.g., [Filippelli and Delaney, 1996](#);
500 [Föllmi et al., 2005](#)).

501 At Riniken, P_{det} is moderately correlated with the detrital index ($r^2= 0.42$), Ti ($r^2=$
502 0.48), Zr ($r^2=0.56$) at the base of the CIE interval. This correlation is not observed at Creux de
503 l’Ours. The paleogeographic position of the Riniken section close to large landmasses
504 coupled with the increase in hydrolysis in the source areas (high CIA*) likely favoured high P
505 input from the continent, boosting primary productivity ([Föllmi, 1995](#); [Tyrell, 1999](#)). In
506 addition, P_{org} recycling (low P_{org} burial efficiency) under reducing conditions during the T-
507 OAE was likely efficient creating a positive feedback loop sustaining primary productivity, as
508 is also known from other OAEs. Therefore, the decrease in P_{org} burial efficiency at Riniken
509 and Creux de l’Ours during the T-OAE likely helped to sustain oxygen depleted conditions.

510 At Breggia (Lombardian basin), low P_{tot} values in the upper portion of the CIE may be
511 related to the (i) large distance away from large landmasses, which limited the export of
512 nutrients, (ii) the more arid climate prevailing along the southern Tethyan margin ([van de](#)
513 [Schootbrugge et al., 2005](#)), and (iii) low dissolved P concentrations in the water column. The

514 slight increase in P_{tot} values recorded during the CIE interval is likely linked to the low
515 sediment-accumulation rate.

516

517 *5.5. Depositional conditions during the T-OAE across the Alpine Tethys*

518 The mineralogical and geochemical results from the studied sections bring further
519 insights into the T-OAE, with a particular focus on the environmental and depositional
520 conditions. At Gipf, Riniken (northern shelf) and Creux de l'Ours (Sub-Briançonnais basin),
521 the T-OAE interval is marked by a shift towards warmer and more humid conditions
522 associated with an enhanced hydrological cycle and an increase in continental weathering, as
523 it also occurred elsewhere in the central and NW European basins (Cohen et al., 2004; Brazier
524 et al., 2015; Montero-Serrano et al., 2015; Percival et al., 2016). These conditions coupled
525 with the Early Toarcian transgression promoted nutrient input, and this probably also by the
526 reworking of soils and sediments from the continent into the more proximal basins. Therefore,
527 the paleogeographic position of the sites and their distance away from large landmasses
528 played a role in the distribution of continental input, with the northern shelf (i.e., Gipf and
529 Riniken) likely being more sensitive than the Sub-Briançonnais basin (i.e., Creux de l'Ours).
530 The increase in nutrient availability boosted primary productivity at these sites, which
531 favoured the development of oxygen depleted conditions. Reducing conditions developed as a
532 function of the paleogeography and were enhanced by the thermohaline stratification of the
533 water column, as proposed for European basins (Bjerrum et al., 2001; van de Schootbrugge et
534 al., 2005; Mattioli et al., 2008; Dera and Donnadieu, 2012; Fantasia et al., in review).
535 Consequently, the development of oxygen depleted conditions promoted benthic regeneration
536 of organic-bound P and its transfer back into the water column (high $C_{\text{org.}}/P_{\text{org.}}$ ratios),
537 ultimately sustaining primary productivity in a positive feedback loop.

538 At Breggia, the large distance away from landmasses and/or the presence of a more
539 arid climate likely limited the nutrient input by fluvial discharge. Under such conditions, high
540 primary productivity was not favoured and the oxygen-minimum zone likely not expanded
541 into the Lombardian basin, as was previously suggested (Farrimond et al., 1998). The
542 circulation pattern and the morphology of the Lombardian basin controlled the development
543 of oxygen-depleted conditions, which were restricted to the deepest parts of the basin
544 (Farrimond et al., 1989). This supports previous interpretations that nutrient concentrations
545 were different between the northern and southern Tethyan margin (e.g., Farrimond et al.,
546 1989; van de Schootbrugge et al., 2005; Reolid et al., 2014).

547 The studied transect provide further evidence that the onset of the Karoo-Ferrar LIP
548 triggered the profound environmental perturbations associated with the T-OAE and that local
549 conditions modulated the response to this global event (e.g., Cohen et al., 2004; McElwain et
550 al., 2005; McArthur et al., 2008; Hermoso et al., 2009). It is currently thought that the
551 termination of the T-OAE was related to the drawdown of excessive atmospheric CO₂ through
552 enhanced continental weathering and increased organic-carbon burial in the marine realm,
553 thus diminishing the greenhouse effects (Jenkyns, 2003). However, this may be questioned
554 since several sections recording the T-OAE CIE lack significant OM content (e.g., Wignall et
555 al., 2005; McArthur et al., 2008). In addition, most European sections, where high organic-
556 carbon contents are recorded, show relatively low average organic-carbon burial rates (Suan
557 et al., 2016), when compared to modern high-productivity sites (Föllmi et al., 2005). In
558 analogy to Suan et al. (2016), organic-carbon burial rates were calculated for the T-OAE
559 interval at Riniken and Creux de l'Ours, using average TOC contents (Riniken: 5.9 wt.%,
560 Creux de l'Ours: 4.5 wt.%), an average density for marly sediments of 1.7 g/cm³, and a
561 duration for the core of the negative CIE of 450 kyrs (Suan et al., 2008; Ruebsam et al., 2014)
562 or 200 kyrs (Boulila et al., 2014). Calculated organic-carbon burial rates are relatively low

563 (Riniken: 0.24 and 0.55 g/m²/yr, Creux de l'Ours: 0.57 and 1.29 g/m²/yr) relative to modern
564 high-productivity sites (e.g., Föllmi et al., 2005), questioning the role of such sites as
565 important sinks for atmospheric CO₂, similar to what was observed for the early Aptian
566 OAE1a (Föllmi, 2012). The development of vegetation in European areas owing to more
567 humid conditions (up to the *bifrons* Zone, Dera et al., 2009) may also have acted as a carbon
568 sink (Westermann et al., 2010; Föllmi, 2012). Recently, it was proposed that the increase in
569 humid conditions favoured the development of large organic-rich lake systems, which
570 significantly contributed to the reduction of the *p*CO₂ (Xu et al., 2017). The enhancement of
571 fire activity during the T-OAE, and in particular during its termination, may have played an
572 important role in terminating ocean anoxia (Baker et al., 2017).

573

574 **6. Conclusions**

575 The high-resolution study of five sections recording the CIE provides critical
576 mineralogical and geochemical data, which permit to compare the paleoenvironmental and
577 depositional conditions across the Alpine Tethys during the T-OAE. This transect highlights
578 the different response to the T-OAE depending on the paleogeographic position of the
579 sections, emphasising the importance of local conditions in modulating the impact of the T-
580 OAE. The mineralogical proxies show that the warm and humid climate prevailing during the
581 T-OAE led to increased runoff and higher terrigenous input on the northern shelf and in the
582 Sub-Briançonnais basin. The nutrient distribution was probably governed by the proximity to
583 continental masses and likely favoured productivity-driven anoxia in the proximal and more
584 restricted settings. The redox-sensitive TEs show a gradient across the studied transect. Gipf
585 and Riniken (northern shelf) were characterised by dysoxic to anoxic conditions, whereas less
586 reducing conditions were present at Creux de l'Ours (Sub-Briançonnais) and oxic conditions

587 at Breggia (Lombardian basin). Thermohaline stratification promoted reducing conditions and
588 the preservation of the organic matter on the northern shelf and in the Sub-Briançonnais
589 basin. Under such conditions, the release of phosphorus from the sediments into the water
590 column likely sustained the primary productivity, acting as a positive feedback loop. At
591 Breggia, the remote position away from large landmasses and/or the prevalence of low
592 hydrolysing conditions on the continents adjacent to the southern Tethys precluded high
593 nutrient input rates and the resulting primary productivity was low.

594

595 **Acknowledgements**

596 This research is supported by the Swiss National Science Foundation (project 200021-
597 1495461/1) and the GeoNova project. We acknowledge the NAGRA and the Cantonal
598 Museum of Natural History (Lugano) for their permission to collect samples from the Riniken
599 core and Breggia section, respectively. We would like to thank Jean-Claude Lavanchy and
600 Tiffany Monnier (Institut des Sciences de la Terre, UNIL) for the XRF analyses and help in
601 the laboratory. We acknowledge Matías Reolid and one anonymous reviewer for their
602 constructive review.

603

604 **References**

- 605 Abed, A.M., Sadaqah, R.M., 2013. Enrichment of uranium in the uppermost Al-Hisa
606 Phosphorite Formation, Eshidiyya basin, southern Jordan. *Journal of African Earth*
607 *Sciences*, 77, 31-40.
- 608 Adatte, T., Stinnesbeck, W., Keller, G., 1996. Lithostratigraphic and mineralogic correlations
609 of near K/T boundary clastic sediments in northeastern Mexico: implications for
610 origin and nature of deposition. *Geol. Soc. Am. Spec. Pap.* 307, 211–226.

- 611 Adatte, T., Keller, G., Stinnesbeck, W., 2002. Late Cretaceous to early Paleocene climate and
612 sea-level fluctuations: the Tunisian record. *Palaeogeogr. Palaeoclimatol. Palaeoecol.*,
613 178, 165–196
- 614 Algeo, T. and Ingall, E., 2007. Sedimentary $C_{org}:P$ ratios, paleocean ventilation and
615 Phanerozoic atmospheric pO_2 . *Palaeogeogr. Palaeoclimatol. Palaeoecol.*, 256, 130–
616 155.
- 617 Algeo, T.J., Maynard, J.B., 2004. Trace-element behavior and redox facies in core shales of
618 Upper Pennsylvanian Kansas-type cyclothems. *Chem. Geol.* 206, 289–318.
- 619 Algeo, T.J., and Tribovillard, N., 2009. Environmental analysis of paleoceanographic systems
620 based on molybdenum-uranium covariation. *Chem. Geol.*, 211-225.
- 621 Al-Suwaidi, A.H., Hesselbo, S.P., Damborenea, S.E., Manceñido, M.O., Jenkyns, H.C.,
622 Riccardi, A.C., Angelozzi, G.N., Baudin, F., 2016. The Toarcian Oceanic Anoxic
623 Event (Early Jurassic) in the Neuquén Basin, Argentina: A reassessment of age and
624 carbon isotope stratigraphy. *The Journal of Geology*, volume 124.
- 625 Anderson, L.D., Delaney, M.L., Faul, K.L., 2001. Carbon to phosphorus ratios in sediments:
626 Implications for nutrient cycling. *Global Biogeochem. Cycles*, vol. 15, No. 1, 65-79.
- 627 Baudin, F., Herbin, J.P., Vandenbroucke, M., 1990. Mapping and geochemical
628 characterization of the Toarcian organic matter in the Mediterranean Tethys and
629 Middle East. *Org. Geochem*, 16, 677-687.
- 630 Baker, S.J., Hesselbo, S.P., Lenton, T.M., Duarte, L.V., Belcher, C.M., 2017. Charcoal
631 evidence that rising atmospheric oxygen terminated Early Jurassic ocean anoxia.
632 *Nature communications*, 8, 15018.
- 633 Behar, F., Beaumont, V. and Penteadó, H.L.D., 2001. Rock-Eval 6 technology: performances
634 and developments. *Oil and Gas Sci. and Tech.*, 56 (2), 111–134.
- 635 Bernoulli, D., Ulmer, P., 2016. Dropstones in Rosso Ammonitico-facies pelagic sediments of
636 the Southern Alps (southern Switzerland and northern Italy). *Swiss J. Geosci.* 109, 57-
637 67.

- 638 Bjerrum, C.J., Surlyk, F., Callomon, J.H., Singerland, R.L., 2001. Numerical
639 Paleooceanographic study of the Early Jurassic transcontinental Laurasian Seaway.
640 *Paleoceanography*, 16, 390-404.
- 641 Blomeier, D.P.G., Reijmer, J.J.G., 1999. Drowning of a Lower Jurassic Carbonate Platform:
642 Jbel Bou Dahar, High Atlas, Morocco. *Facies* 41, 81-110.
- 643 Bodin, S., Krencker, F.N., Kothe, T., Hoffmann, R., Mattioli, E., Heimhofer, U. and Kabiri,
644 L., 2016. Perturbation of the carbon cycle during the late Pliensbachian-early
645 Toarcian: New insight from high-resolution carbon isotope records in Morocco. *J. Afr.*
646 *Earth Sci.*, 116, 89-104.
- 647 Bond, D.P.G., Wignall, P.B., 2014. Large igneous provinces and mass extinctions: an update.
648 In: Keller, G., Kerr, A.C. (Eds.), *Impacts and Mass Extinction: Causes and Effects*. In:
649 *Spec. Pap., Geol. Soc. Am.*, vol.505, pp.29–55.
- 650 Bougeault, C., Pellenard, P., Deconinck, J.-F., Hesselbo, S. P., Dommergues, J.-L., Bruneau,
651 L., Cocquerez, T., Laffont, R., Huret, E., Thibault, N., 2017. Climatic and
652 palaeoceanographic changes during the Pliensbachian (Early Jurassic) inferred from
653 clay mineralogy and stable isotope (C-O) geochemistry (NW Europe). *Global Planet.*
654 *Change*, 149, 139-152.
- 655 Boulila, S., Galbrun, B., Huret, E., Hinnov, L.A., Rouget, I., Gardin, S. and Bartolini, A.,
656 2014. Astronomical calibration of the Toarcian Stage: Implications for sequence
657 stratigraphy and duration of the early Toarcian OAE. *Earth Planet. Sci. Lett.*, 386, 98–
658 111.
- 659 Brazier, J.-M., Suan, G., Tacail, T., Simon, L., Martin, J. E., Mattioli, E., Balter, V., 2015.
660 Calcium isotope evidence for dramatic increase of continental weathering during the
661 Toarcian oceanic anoxic event (Early Jurassic), *Earth Planet. Sci. Lett.*, 411, 164–176.
- 662 Brumsack, H.-J., 1991. Inorganic geochemistry of the German Posidonia Shale:
663 paleoenvironmental consequences. In: Tyson, R.V., Pearson, T.H. (Eds.), *Modern and*
664 *ancient continental shelf anoxia*. Geological Society, London, Special Publications 58,
665 pp. 353–362.

- 666 Brumsack, H.J., 2006. The trace metal content of recent organic carbon-rich sediments:
667 implications for Cretaceous black shale formation. *Palaeogeogr. Palaeoclimatol.*
668 *Palaeoecol.*, 232, 344–361.
- 669 Burgess, S.D., Bowring, S.A., Fleming, T.H., Elliot, D.H., 2015. High-precision
670 geochronology links the Ferrar large igneous province with early-Jurassic ocean
671 anoxia and biotic crisis. *Earth Planet. Sci. Lett.* 415, 90–99.
- 672 Burtner, R.L., Warner, M.A., 1986. Relationship between illite/smectite diagenesis and
673 hydrocarbon generation in Lower Cretaceous Mowry and Skull Creek Shales of the
674 northern Rocky Mountain area. *Clay Clay Mineral.*, 34, 390–402.
- 675 Calvert, S.E., Pedersen, T.F., 2007. Elemental proxies for palaeoclimatic and
676 palaeoceanographic variability in marine sediments: interpretation and application. In:
677 Hillaire-Marcel, C., Vernal, A.D. (Eds.), *Proxies in Late Cenozoic Paleooceanography*.
678 Elsevier, Amsterdam, 567–644.
- 679 Caruthers, A.H., Gröcke, D.R., Smith, P.L., 2011. The significance of an Early Jurassic
680 (Toarcian) carbon-isotope excursion in Haida Gwaii (Queen Charlotte Islands), British
681 Columbia, Canada. *Earth Planet. Sci. Lett.* 307, 19–26.
- 682 Chamley, H., 1989. *Clay Sedimentology*. Springer Verlag, Berlin.
- 683 Cohen, A.S., Coe, A.L., Harding, S.M., Schwark, L., 2004. Osmium isotope evidence for the
684 regulation of atmospheric CO₂ by continental weathering. *Geology* 32, 157–160.
- 685 Deconinck, J.-F., Bernoulli, D., 1991. Clay mineral assemblages of Mesozoic pelagic and
686 flysch sediments of the Lombardian Basin (Southern Alps): implications for
687 palaeotectonics, palaeoclimate and diagenesis. *Geol. Rundsch.* 80, 1–17.
- 688 Dera, G., Pellenard, P., Neige, P., Deconinck, J.-F., Pucéat, E., Dommergues, J.-L., 2009.
689 Distribution of clay minerals in Early Jurassic Peritethyan seas: palaeoclimatic
690 significance inferred from multiproxy comparisons. *Palaeogeogr. Palaeoclimatol.*
691 *Palaeoecol.*, 271, 39–51.
- 692 Dera, G., Donnadiou, Y., 2012. Modeling evidences for global warming, Arctic seawater
693 freshening, and sluggish oceanic circulation during the Early Toarcian anoxic event.
694 *Paleoceanography*, 27, PA2211.

695 Duchamp-Alphonse, S., Fiet, N., Adatte, T., Pagel, M., 2011. Climate and sea-level variations
696 along the northwestern Tethyan margin during the Valanginian C-isotope excursion:
697 mineralogical evidence from the Vocontian Basin (SE France). *Palaeogeogr.*
698 *Palaeoclimatol. Palaeoecol.*, 302, 243–254.

699 Eaton, A.D., Clasceri, L.S., Greenberg, A.E., 1995. *Standard Methods for the Examination of*
700 *Water and Waste Water*, vol. IXI 4.113–4.114.

701 Fantasia, A., Föllmi, K.B., Adatte, T., Spangenberg, J.E., Mattioli, E. (in review). Expression
702 of the Early Toarcian oceanic anoxic event: New insights from a Swiss transect. In
703 review in *Sedimentology*.

704 Farrimond, P., Eglinton, G., Brassell, S.C., Jenkyns, H.C., 1989. Toarcian anoxic event in
705 Europe: an organic geochemical study. *Mar. Petrol. Geol.*, 6, 136-147.

706 Fedo, C., Nesbitt, H.W., Young, G.M., 1995. Unravelling the effects of potassium
707 metasomatism in sedimentary rocks and paleosols, with implications for
708 paleoweathering conditions and provenance. *Geology*, 23, 921-924.

709 Ferreira, J., Mattioli, E., Pittet, B., Cachão, M., Spangenberg, J.E., 2017. Palaeoecological
710 insights on Toarcian and lower Aalenian calcareous nannofossils from the Lusitanian
711 Basin (Portugal). *Palaeogeogr. Palaeoclimatol. Palaeoecol.*, 436, 245-262.

712 Filippelli, G.M., Delaney, M.L., 1996. Phosphorus geochemistry of equatorial Pacific
713 sediments. *Geochim. Cosmochim. Acta*, 60, 1479-1495.

714 Föllmi, K.B., 1996. The phosphorus cycle, phosphogenesis and marine phosphate-rich
715 deposits. *Earth-Sci. Rev.*, 40, 55-124.

716 Föllmi, K.B., de Kaenel, E., Stille, P., John, C.M., Adatte, T., Steinmann, P., 2005.
717 Phosphogenesis and organic-carbon preservation in the Miocene Monterey Formation
718 at Naples Beach, California-The Monterey hypothesis revisited. *GSA Bulletin*, 117,
719 589-619.

720 Fu, X., Wang, J., Zeng, S., Feng, X., Wang, D., Song, C., 2017. Continental weathering and
721 paleoclimatic changes through the onset of the Early Toarcian oceanic anoxic event in
722 Qiangtang Basin, eastern Tethys. *Palaeogeogr. Palaeoclimatol. Palaeoecol.*, 302, 487,
723 241-250.

- 724 Gibbs, R.J., 1977. Clay-mineral segregation in the marine environment. *J. Sediment. Petrol.*
725 47, 237–243.
- 726 Godet, A., Bodin, S., Adatte, T., Föllmi, K.B., 2008. Platform-induced clay-mineral
727 fractionation along a northern Tethyan basin-platform transect: implications for the
728 interpretation of Early Cretaceous climate change (Late Hauterivian–Early Aptian).
729 *Cretac. Res.* 29, 830–847.
- 730 Gröcke, D.R., Hori, R.S., Trabucho-Alexandre, J., Kemp, D.B., Schwark, L., 2011. An open
731 ocean record of the Toarcian oceanic anoxic event. *Solid Earth* 2, 245–257.
- 732 Haq, B.U., Hardenbol, J., Vail, P.R., 1987. Chronology of fluctuating sea levels since the
733 Triassic. *Science* 235, 1156–1167.
- 734 Haq, B, U., 2017. Jurassic Sea-Level Variations: A Reappraisal. *Geological Society of*
735 *America*, 18 (1).
- 736 Hardenbol, J., Thierry, J., Farley, M.B., de Graciansky, P.-C. and Vail, P.R., 1998. Mesozoic
737 and Cenozoic sequence chronostratigraphic framework of European basins. In: de
738 Graciansky, P.-C., Hardenbol, J., Jacquin, T., Vail, P.R. (Eds.), *Mesozoic and*
739 *Cenozoic Sequence Stratigraphy of European basins*. *SEPM Spec. Publ.*, 60, 3–13.
- 740 Harries, P.J. and Little, C.T.S., 1999. The early Toarcian (Early Jurassic) and the
741 Cenomanian–Turonian (Late Cretaceous) mass extinctions: similarities and contrasts.
742 *Palaeogeogr. Palaeoclimatol. Palaeoecol.*, 154, 39–66.
- 743 Hermoso, M., Minoletti, F., Le Callonnec, L., Jenkyns, H.C., Hesselbo, S.P., Rickaby,
744 R.E.M., Renard, M., de Rafélis, M. and Emmanuel, L., 2009. Global and local forcing
745 of Early Toarcian seawater chemistry: a comparative study of different
746 paleoceanographic settings (Paris and Lusitanian basins). *Paleoceanography*, 24, 1–15.
- 747 Hermoso, M., Minoletti, F., Rickaby, R.E.M., Hesselbo, S.P., Baudin, F., Jenkyns, H.C.,
748 2012. Dynamics of a stepped carbon-isotope excursion: Ultra high-resolution study of
749 Early Toarcian environmental change. *Earth Planet. Sci. Lett.*, 319–320, 45–54.
- 750 Hermoso, M. and Pellenard, P., 2014. Continental weathering and climatic changes inferred
751 from clay mineralogy and paired carbon isotopes across the early to middle Toarcian
752 in the Paris Basin. *Palaeogeogr. Palaeoclimatol. Palaeoecol.*, 399: 385–393.

- 753 Hesselbo, S.P., Jenkyns, H.C., Duarte, L.V., Oliveira, L.C.V., 2007. Carbon-isotope record of
754 the Early Jurassic (Toarcian) Oceanic Anoxic Event from fossil wood and marine
755 carbonate (Lusitanian Basin, Portugal). *Earth Planet. Sci. Lett.*, 253, 455–470.
- 756 Jenkyns, H.C., 1988. The early Toarcian (Jurassic) anoxic event; stratigraphic, sedimentary
757 and geochemical evidence. *Am. J. Sci.*, 288, 101–151.
- 758 Jenkyns, H.C., Gröcke, D.R., Hesselbo, S.P., 2001. Nitrogen isotope evidence for water mass
759 denitrification during the early Toarcian (Jurassic) oceanic anoxic event.
760 *Paleoceanography*, 16, 593-603.
- 761 Jenkyns, H.C., 2003. Evidence for rapid climate change in the Mesozoic–Palaeogene
762 greenhouse world, *Philos. Trans. R. Soc. London, Ser. A*, 361, 1885–1916.
- 763 Jenkyns, H.C., 2010. Geochemistry of oceanic anoxic events. *Geochem. Geophys. Geosyst.*
764 11.
- 765 Kemp, D.B., Coe, A.L., Cohen, A.S., Weedon, G.P., 2011. Astronomical forcing and
766 chronology of the early Toarcian (Early Jurassic) oceanic anoxic event in Yorkshire,
767 UK. *Paleoceanography*, 26.
- 768 Kemp, D.B., Izumi, K., 2014. Multiproxy geochemical analysis of a Panthalassic margin
769 record of the early Toarcian oceanic anoxic event (Toyora area, Japan). *Palaeogeogr.*
770 *Palaeoclimatol. Palaeoecol.*, 414: 332-341.
- 771 Klug, H.P., Alexander, L., 1974. *X-ray Diffraction Procedures for Polycrystalline and*
772 *Amorphous Materials*. John Wiley and Sons, Inc. First and Second editions, New
773 York.
- 774 Kuhn, O. and Etter, W., 1994. Der Posidonienschiefer der Nordschweiz: Lithostratigraphie,
775 Biostratigraphie, Fazies. *Eclogae Geol. Helv.* 87/1, 113-138.
- 776 Kübler, B., 1983. Cristallinité de l'illite, méthodes normalisées de préparations, méthodes
777 normalisées de mesures. *Cahiers Institut Géologie de Neuchâtel, Suisse (série ADX)*.
- 778 Kübler, B., 1987. Cristallinité de l'illite : méthode normalisée de préparation de mesure,
779 méthode automatique normalisée de mesure. *Cahiers de l'Institut de Géologie, Séries*
780 *AX*, 3.1 and 3.2, 1–3.

- 781 Kübler, B., Jaboyedoff, M., 2000. Illite crystallinity. *Comptes Rendus de l'Académie des*
782 *Sciences Paris Sciences de la Terre et des planètes série ADX 1*, 1–13. *Earth and*
783 *Planetary Sciences* 331, 75–89.
- 784 Lanson, B., Beaufort, D., Berger, G., Bauer, A., Cassagnabere, A., Meunier, A., 2002.
785 Authigenic kaolin and illitic minerals during burial diagenesis of sandstones: a review.
786 *Clay Minerals* 37, 1–22.
- 787 Matter, A., Peters, T., Isenschmid, C., Bläsi, H.R. and Ziegler, H.-J., 1987. Sondierbohrung
788 Riniken – Geologie. Nagra Tech. Ber., 86-02, Nagra, Wettingen.
- 789 Mattioli, E., Pittet, B., Petitpierre, L., Mailliot, S., 2009. Dramatic decrease of pelagic
790 carbonate production by nannoplankton across the Early Toarcian anoxic event (T-
791 OAE), *Global Planet. Change*, 65(3–4), 134–145.
- 792 McArthur, J.M., Algeo, T.J., van de Schootbrugge, B., Li, Q., and Howarth, R.J., 2008.
793 Basinal restrictions, black shales, Re-Os dating, and the early Toarcian (Jurassic)
794 oceanic anoxic event. *Paleoceanography*, 23(4).
- 795 McElwain, J.C., Wade-Murphy, J., Hesselbo, S.P., 2005. Changes in carbon dioxide during an
796 oceanic anoxic event linked to intrusion into Gondwana coals. *Nature* 435, 479–482.
- 797 McLennan, S.M., 1993. Weathering and global denudation. *Journal of Geology* 101, 295–
798 303.
- 799 McLennan, S.M., Hemming, S., McDaniel, D.K., Hanson, G.N., 1993. Geochemical
800 approaches to sedimentation, provenance and tectonics. *Geol. Soc. Am. Spec. Pap.*
801 284.
- 802 Mettraux M., Mosar J., 1989. Tectonique alpine et paléotectonique liasique dans les Préalpes
803 Médiannes en rive droite du Rhône. *Eclogae geol. Helv.*, 82. 517-540.
- 804 Montero-Serrano, J.-C., Föllmi, K.B., Adatte, T., Spangenberg, J.E., Tribovillard, N.,
805 Fantasia, A., Suan, G., 2015. Continental weathering and redox conditions during the
806 early Toarcian Oceanic Anoxic Event in the northwestern Tethys: Insight from the
807 Posidonia Shale section in the Swiss Jura Mountains. *Palaeogeogr. Palaeoclimatol.*
808 *Palaeoecol.*, 429, 83–99.

- 809 Mort, H., Adatte, T., Föllmi, K.B, Keller, G., Steinmann, P., Matera, V., Berner, Z., Stüben,
810 D., 2007. Phosphorus and the roles of productivity and nutrient recycling during
811 Oceanic Anoxic Event 2. *Geology* 35–6, 483–486.
- 812 Nesbitt, H.W., Young, G.M., 1989. Formation and diagenesis of weathering profiles. *J.*
813 *Geol.*97 (2), 129–147.
- 814 Nordstrom, D.K., Aqueous pyrite oxidation and the consequent formation of secondary iron
815 minerals. In: Kittrick JA, Fanning DF, Hossner LR (eds) *Acid sulfate weathering:*
816 *pedogeochemistry and relationship to manipulation of soil materials.* Soil Science
817 Society of America, 37–56.
- 818 Pálffy, J. and Smith, P.L., 2000. Synchrony between Early Jurassic extinction, oceanic anoxic
819 event, and the Karoo-Ferrar flood basalt volcanism. *Geology*, 28, 747–750.
- 820 Percival, L.M.E., Cohen, A.S., Davies, M.K., Dickson, A.J., Hesselbo, S.P., Jenkyns, H.C.,
821 Leng, M.J., Mather, T.A., Storm, M.S., Xu, W., 2016. Osmium isotope evidence for
822 two pulses of increased continental weathering linked to Early Jurassic volcanism and
823 climate change. *Geology*, 44, 759-762.
- 824 Redfield, A.C., 1958. The biological control of chemical factors in the environment. *Am. Sci.*
825 46, 205–222.
- 826 Reolid, M., 2014. Stable isotopes on foraminifera and ostracods for interpreting incidence of
827 the Toarcian Oceanic Anoxic Event in Westernmost Tethys: Role of water stagnation
828 and productivity. *Palaeogeogr. Palaeoclimatol. Palaeoecol.*, 395, 77-91.
- 829 Reolid, M., Mattioli, E., Nieto, L.M., Rodríguez-Tovar, F., 2014. The Early Toarcian Oceanic
830 Anoxic Event in the External Subbetic (Southiberian Palaeomargin, Westernmost
831 Tethys): Geochemistry, nannofossils and ichnology. *Palaeogeogr. Palaeoclimatol.*
832 *Palaeoecol.*, 411, 79-94.
- 833 Rieber, H., 1973. Fauna und Stratigraphie einer oolithischen Kalkbank aus dem Toarcium von
834 Gipf (Kanton Aargau, Schweiz). *Eclogae Geol. Helv.* 66/3, 657-665.
- 835 Riquier, L., Tribovillard, N., Averbuch, O., Devleeschouwer, X., Riboulleau, A., 2006. The
836 Late Frasnian Kellwasser horizons of the Harz Mountains (Germany): two oxygen
837 deficient periods resulting from different mechanisms. *Chem. Geol.* 233, 137–155.

- 838 Röhl, H.J., Schmid-Röhl, A., Oschmann, W., Frimmel, A. and Schwark, L., 2001. The
839 Posidonia Shale (Lower Toarcian) of SW-Germany: an oxygen-depleted ecosystem
840 controlled by sea level and palaeoclimate. *Palaeogeogr. Palaeoclimatol. Palaeoecol.*,
841 165, 27–52.
- 842 Ruttenberg, K.C., 1992. Development of a sequential extraction method for different forms of
843 phosphorus in marine sediments: *Limnol. Oceanogr.*, 37, 1460-1482.
- 844 Schenau, S.J., de Lange, G.J., 2000. A novel chemical method to quantify fish debris in
845 marine sediments. *Limnol. Oceanogr.*, 45, 963-971.
- 846 Singer, A., 1984. The palaeoclimatic interpretation of clay minerals in sediments – a review.
847 *Earth Science Review*, 21, 251–293.
- 848 Slomp, C.P., Epping, E.H.G., Helder, W., Van Raaphorst, W., 1996. A key for iron-bound
849 phosphorus in authigenic apatite formation in North Atlantic continental platform
850 sediments. *J. Mar. Res.*, 54, 1179-1205.
- 851 Suan, G., Pittet, B., Bour, I., Mattioli, E., Duarte, L.V. and Mailliot, S., 2008. Duration of the
852 Early Toarcian carbon isotope excursion deduced from spectral analysis: Consequence
853 for its possible causes. *Earth Planet. Sci. Lett.*, 267, 666–679.
- 854 Suan, G., Nikitenko, B.L., Rogov, M.A., Baudin, F., Spangenberg, J.E., Knyazev, V.G.,
855 Glinskikh, L.A., Goryacheva, A.A., Adatte, T., Riding, J.B., Föllmi, K.B., Pittet, B.,
856 Mattioli, E., Lécuyer, C., 2011. Polar record of Early Jurassic massive carbon
857 injection. *Earth Planet. Sci. Lett.*, 312, 102–113.
- 858 Suan, G., van de Schootbrugge, B., Adatte, T., Fiebig, J. and Oschmann, W., 2015.
859 Calibrating the magnitude of the Toarcian carbon cycle perturbation.
860 *Paleoceanography*, 30, 495–509.
- 861 Suan, G., Schlögl, J., Mattioli, E., 2016. Bio-and chemostratigraphy of the Toarcian organic-
862 rich deposits of some key successions of the Alpine Tethys. *Newsletters on*
863 *Stratigraphy*, 49/3, 401-419.
- 864 Svensen, H., Planke, S., Chevallier, L., Malthe-Sørensen, A., Corfu, F., Jamtveit, B., 2007.
865 Hydrothermal venting of greenhouse gases triggering Early Jurassic global warming.
866 *Earth Planet. Sci. Lett.*, 256, 554–566.

- 867 Them II, T. R., Gill, B.C., Caruthers, A.H., Gröcke, D.R., Tulsy, E.T., Martindale, R.C.,
868 Poulton, T.P., Smith, P.L., 2017. High-resolution carbon isotope records of the
869 Toarcian Oceanic Anoxic Event (Early Jurassic) from North America and implications
870 for the global drivers of the Toarcian carbon cycle. *Earth Planet. Sci. Lett.*, 459, 118–
871 126.
- 872 Thierry, J., 2000. Late Toarcian. In: Dercourt, J., Gaetani, M., Vrielynck, B., Barrier, E., Biju-
873 Duval, B., Brunet, M.F., Cadet, J.P., Crasquin, S., Sandulescu, M. (Eds.), *Atlas Peri-
874 Tethys. Palaeogeographical Maps.*
- 875 Thiry, M., 2000. Palaeoclimatic interpretation of clay minerals in marine deposits: an outlook
876 from the continental origin. *Earth-Sci. Rev.*, 49, 201–221.
- 877 Todorov I., Schegg, R., Wildi, W., 1993. Thermal maturity and modelling of Mesozoic and
878 Cenozoic sediments in the south of the Rhine Graben and the Eastern Jura
879 (Switzerland). *Eclogae Geol. Helv.*, 86/3, 667–692.
- 880 Trecalli, A., Spangenberg, J.E., Adate, T., Föllmi, K.B., Parente, M., 2012. Carbonate
881 platform evidence of ocean acidification at the onset of the early Toarcian oceanic
882 anoxic event. *Earth Planet. Sci. Lett.*, 357–358, 214–225.
- 883 Tribouillard, N., Algeo, T.J., Lyons, T., Riboulleau, A., 2006. Trace metals as paleoredox and
884 paleoproductivity proxies: an update. *Chem. Geol.*, 232 (1–2), 12–32.
- 885 Tröster, J., 1987. Biostratigraphie des Obertoarcium und der Toarcium/Aalenium-Grenze der
886 Bohrungen Weiach, Beznau, Riniken und Schafisheim (Nordschweiz). *Eclogae Geol.
887 Helv.*, 80, 431–447.
- 888 Tyrell, T., 1999. The relative influences of nitrogen and phosphorus on oceanic primary
889 production. *Nature*, 400, 525–531.
- 890 Van Cappellen, P., Ingall, E.D., 1994. Benthic phosphorus regeneration, net primary
891 production, and ocean anoxia: a model of the coupled marine biogeochemical cycles
892 of carbon and phosphorus. *Paleoceanography*, 9, 677–692.
- 893 Van de Schootbrugge, B., McArthur, J.M., Bailey, T.R., Rosenthal, J.D., Wright, J.D. and
894 Miller, K.G., 2005. Toarcian oceanic anoxic event: An assessment of global causes
895 using belemnite C isotope records. *Paleoceanography*, 29, 1–10.

- 896 Velde, B., 1995. Origin and mineralogy of clays. *Clays and the Environment*. Springer Verlag
897 (334 pp.).
- 898 Wedepohl, K.H., 1971. Environmental influences on the chemical composition of shales and
899 clays. In: Ahrens, L.H., Press, F., Runcorn, S.K., Urey, H.C. (Eds.), *Physics and*
900 *Chemistry of the Earth*. Pergamon, Oxford, pp. 307–331.
- 901 Westermann, S., Föllmi, K.B., Adatte, T., Matera, V., Schnyder, J., Fleitmann, D., Fiet, N.,
902 Ploch, I., Duchamp-Alphonse, S., 2010. The Valanginian $\delta^{13}\text{C}$ excursion may not be
903 an expression of a global oceanic anoxic event. *Earth Planet. Sci. Lett.*, 290, 118-131.
- 904 Westermann, S., Duchamp-Alphonse, S., Fiet, N., Fleitmann, D., Matera, V., Adatte, T.,
905 Föllmi, K.B., 2013. Paleoenvironmental changes during the Valanginian: New insights
906 from variations in phosphorus contents and bulk-and clay mineralogies in the western
907 Tethys. *Palaeogeogr. Palaeoclimatol. Palaeoecol.*, 392, 196-208.
- 908 Wiedenmayer, F., 1980. Die Ammoniten der Mediterranen Provinz im Pliensbachian und
909 unteren Toarcian aufgrund neuer Untersuchungen im Generoso-Becken
910 (Lombardische Alpen). *Denkschriften der Schweizerischen Naturforschenden*
911 *Gesellschaft*, 93, 263 pp.
- 912 Wignall and Maynard, 1993. The sequence stratigraphy of transgressive black shales
913 B. Katz, L.M. Pratt (Eds.), *Source rocks in a sequence stratigraphic frame work*
914 *AAPG Studies in Geology*, vol. 37, 1993, 35-47.
- 915 Wignall, P.B., Newton, R.J., Little, C.T.S., 2005. The timing of paleoenvironmental change
916 and cause-and-effect relationships during the Early Jurassic mass extinction in Europe.
917 *Am. J. Sci.* 305, 1014–1032.
- 918 Winterer, E.L., Bosellini, A., 1981. Subsidence and sedimentation on Jurassic passive
919 continental margin, Southern Alps, Italy. *AAPG Bull.*, 65, 394–421.
- 920 Xu, W., Ruhl, M., Jenkyns, H.C., Hesselbo, S.P., Riding, J.B., Selby, D., Naafs, B.D.A.,
921 Weijers, J.W.H., Pancost, R., Tegelaar, E. and Idiz, E.F., 2017. Carbon sequestration
922 in an expanded lake system during the Toarcian oceanic anoxic event. *Nature*
923 *Geoscience*, 10, 129-135.
- 924